Supporting Information

Nanosecond timescale motions in proteins revealed by high-resolution NMR relaxometry

Cyril Charlier,[†,‡] Shahid Nawaz Khan,[†,‡] Thorsten Marquardsen,[§] Philippe Pelupessy,[†] Volker Reiss,[§] Dimitris Sakellariou,[†,∥] Geoffrey Bodenhausen,[†,⊥] Frank Engelke,[§] and Fabien Ferrage*[,†]

[†]*Ecole Normale Supérieure, Département de Chimie, UMR 7203 CNRS-UPMC-ENS, Laboratoire des Biomolécules, 24 rue Lhomond, 75231 Paris Cedex 05, France*

[§]*Bruker BioSpin GmbH, Silberstreifen 4, D 76287 Rheinstetten, Germany*

[∥] *Laboratoire Structure et Dynamique par Résonance Magnétique, UMR 3299-SIS2M CEA/CNRS, IRAMIS, DSM, CEA Saclay, F-91191, Gif-sur-Yvette Cedex, France*

[⊥]*Institut des Sciences et Ingénierie Chimiques, Ecole Polytechnique Fédérale de Lausanne, BCH, 1015 Lausanne, Switzerland*

[1] Corresponding author:

Fabien.Ferrage@ens.fr

Tel: +33 1 44 32 33 43

Table of contents

1. DETAILED PRESENTATION OF THE SHUTTLE SYSTEM 3
PROBE 3
SHUTTLE TRANSFER SYSTEM 4
SHUTTLE CONTROLLER UNIT 5
SHUTTLE CONTAINER 6
2. TEMPERATURE CONTROL 7
3. THE ICARUS PROTOCOL 8
SPECTRAL DENSITY FUNCTIONS 8
SPIN SYSTEM 9
FIRST STEP OF ICARUS 11
ITERATIVE ANALYSIS WITH ICARUS 12
ERROR EVALUATION 14
GRAPHICAL OUTPUT 14
4. ORDER PARAMETERS AND TIMESCALES OF MOTIONS 16
ORDER PARAMETERS 16
TIMESCALES OF LOCAL MOTIONS 17
TRANSVERSE RELAXATION 18
COMPARISON OF ORDER PARAMETERS 19
EFFECTIVE DISTANCE TO NEIGHBORING PROTONS 20
5. RELAXATION DATA AND PARAMETERS OF LOCAL DYNAMICS 22
6. REFERENCES 45

1. Detailed presentation of the shuttle system

Probe

The probe uses two coils to generate radiofrequency (*rf*) fields (B_1). We chose saddle coils that allow a vertical shuttle motion of the sample and resemble coils used in standard high-resolution probes. The outer coil is matched to the ^{1}H frequency, in order to minimize mismatching of the ^{1}H channel that may arise from inaccurate positioning of the shuttle and from interactions between the sample and the electric component of the rf field. This outer coil is doubly tuned for ^{1}H (observation) and for ^{2}H (field-frequency lock). The inner coil is doubly tuned for ^{13}C and ^{15}N and oriented in such a manner that the *rf* fields of the inner and outer coils are orthogonal; see Fig. S1 B and C.

Special care was taken (Fig. S1B) to attenuate vibrations arising from shocks when the shuttle is stopped suddenly at the upper and lower ends of its displacement. Careful investigations of these effects were necessary to obtain lineshapes of similar quality as in standard high-resolution NMR spectroscopy. A shielded z-gradient coil (Fig. S1 A and B) allows one to use standard NMR experiments.

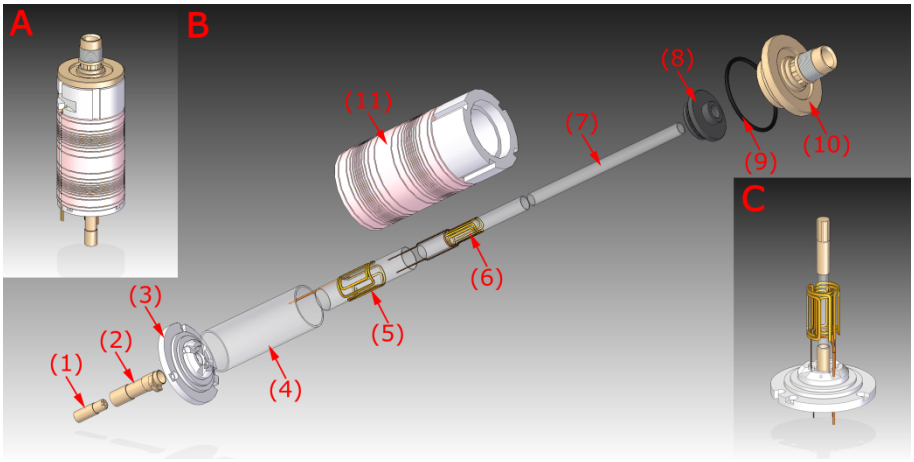

Figure S1: Schematic views of the upper part of the shuttle probe. A. Complete view. B. Exploded view. C. Coil assembly with amorphous quartz shuttle container. (1) Shuttle touchdown pad. (2) Lower attenuating connector. (3) Lower insert. (4) Thermal glass shield. (5) Guiding glass tube and outer *rf* coil. (6) Guiding glass tube and inner *rf* coil. (7) Shuttle protection glass tube. (8) Glass gauge. (9) Vibration damper. (10) Upper insert and second attenuating connector. (11) Z-gradient coil.

A vertical metal tube runs from the bottom of the probe to a position just below the *rf* coils. This tube is used to insert or eject the shuttle container and to guide the shuttle stopper and

the shuttle touchdown pad (Fig. S1B (1) top.) The shuttle stopper is fixed with two springs at the bottom of the coaxial tube. The shuttle stopper and spring serve as shock absorbers that center the shuttle container with respect to the *rf* coils (Fig. S1C). The "lower attenuating connector" marks the transition between the central tube and the detection area at the top of the probe (Fig. S1B (2).) A sensor was integrated in the lower attenuating connector to detect the mechanical position of the shuttle container. A shuttle protection glass tube ensures that the shuttle container is properly aligned (Fig. S1B (7).) The interconnection between the top of the probe and the shuttle transfer system consists of an upper insert and a second attenuating connector (Fig. S1B (10).) An O-ring (Fig. S1B (9)) inserted between the gradient system (Fig. S1B (11)) and the upper insert further improves vibration damping.

The design of the *rf* circuit is similar to many high-resolution probes. Low-susceptibility and/or susceptibility-compensated materials were selected, particularly for the coil and capacitor wires and all surrounding components. As a result, the spectral resolution and line shape were comparable to those of a standard 600 MHz high-resolution probe. However, as expected, the NMR sensitivity of the shuttle probe is reduced by about an order of magnitude due to the lower filling factor and reduced volume of the sample.

Shuttle transfer system

The shuttle transfer system allows one to stop the shuttle at a predetermined position at a chosen height in the stray field above the magnetic center. The shuttle guide consists of a tube connected to the top of the probe at its lower end, and to the top of the cryostat of the main magnet at its upper end. At the top, a second tube, coaxial with the shuttle guide, is equipped with a 'stopper' that prevents the shuttle container to move beyond a well-defined position. This inner tube has been isolated from the outer one and a damping system has been designed to reduce vibrations and shock-waves from the shuttle motion and sudden stop. Inside the stopper a second optical sensor has been integrated to detect the precise position of the shuttle in the low field. The position of the stopper was measured before and after the experiments to ensure that the value of the magnetic field B_0^{low} was constant during the course of the experiment.

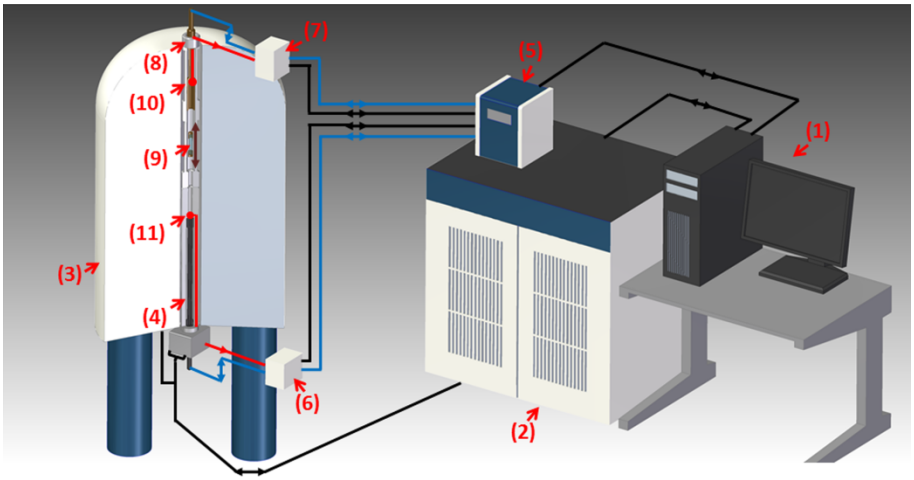

Figure S2: Schematic view of the shuttle system: (1) Workstation; (2) Console; (3) Magnet; (4) Shuttle probe; (5) Main shuttle control; (6) & (7) Shuttle control satellites; (8) Transfer system; (9) Shuttle container; (10) & (11) Optical sensors and touchdown pads.

Shuttle controller unit

The pneumatic shuttle control consists of a main unit and two satellite units (Fig. S2). The main unit is equipped with a microcontroller board which allows communication with the NMR workstation and the spectrometer console, controls the valves and pressures, and allows one to determine the position of the sample. In addition, a pneumatically driven vacuum pump generates a suitable (under) pressure. The two satellites are equipped with a proportional pressure valve that controls the shuttle motion and an optical sensor to detect the end positions of the shuttle. The main unit is designed to be installed either next to the NMR workstation or to the spectrometer console, while the two satellite units should be close to the magnet, one at the bottom, close to the shuttle probe, and the other one at the top, close to the shuttle transfer system.

A simple script file is used to program the shuttle controller. This file lists pressure settings for the transfers and at the two static positions. The pressure settings are kept constant during each phase. The shuttle motion is activated by the TCU (timing control unit) of the spectrometer and information from the optical sensors about the positions (top for low field, bottom for high field) is sent back to the spectrometer. The shuttle controller creates a report in the form of a table with the timing of all shuttle motions that can be displayed by the NMR workstation.

Shuttle container

The shuttle system was developed to withstand fast motions and strong shocks caused by sudden stops. This is particularly important for the sample container (Fig. S3). A special synthetic amorphous quartz was chosen for the glass parts (4) - (7) and a high performance polyimide resin for the caps (1) + (2). Two O-rings (3) were integrated in the caps as dampers to reduce shocks to the glass body. All of these materials have a low magnetic susceptibility to reduce distortions of NMR signals.

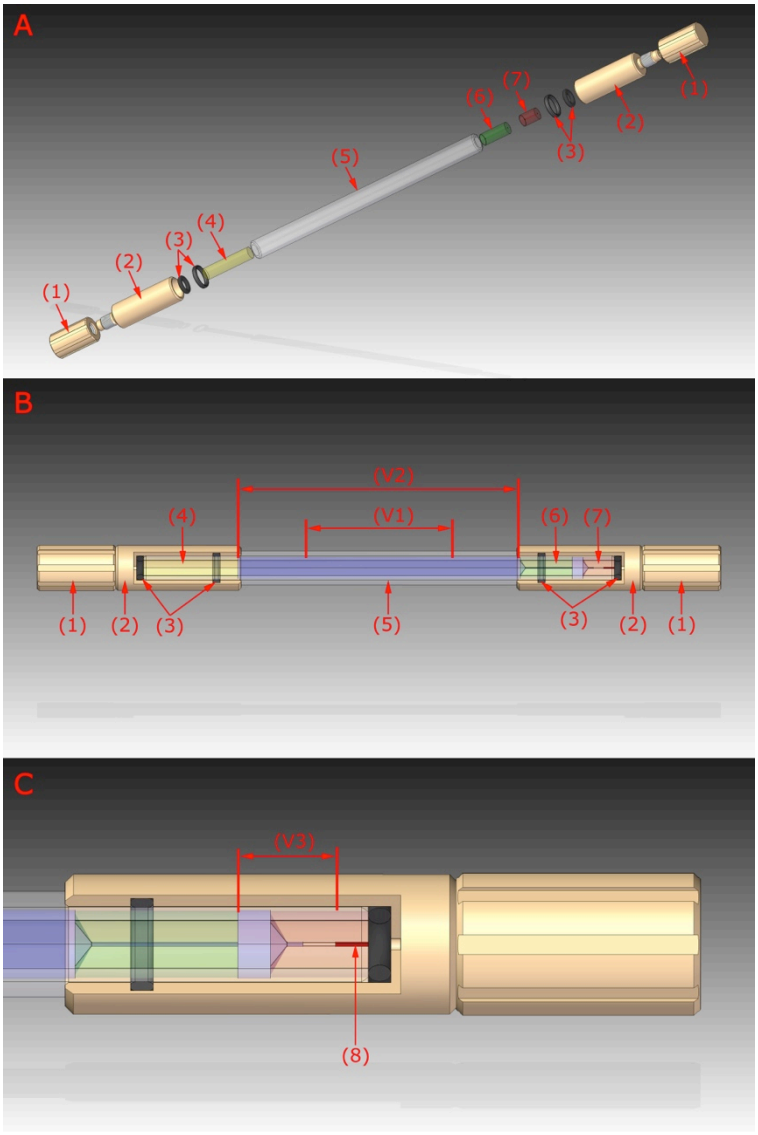

Figure S3: Schematic view of shuttle container. A. Exploded view of all parts; B. Assembled shuttle container with glass parts and sample in blue; (1) End plug; (2) Glass connector; (3) Shock and vibration damper; (4) Bottom glass plug; (5) Shuttle glass tube; (6) Inner glass capillary; (7) Top glass capillary; (V1) active sample volume. (V2) Total sample volume. C. Details of the upper part of the shuttle container: (V3) Sample reservoir and bubble catcher; (8) Glue seal.

The total sample volume (V2) is about is 110 µL, while the active volume (V1) of the sample is about 60 µL. Once filled, the container is sealed with glue. The shuttle container has a "bubble catcher" with a volume of about 10 µL to confine air bubbles that may appear in the sample and to accommodate thermal expansion of the sample. Bubbles appearing in the active volume of the sample can be easily centrifuged into the bubble catcher through a thin capillary. In our hands the samples are stable for several hours, and bubbles are predominantly confined in the bubble catcher.

2. Temperature Control

The sample temperature was monitored using chemical shifts differences of a few selected pairs of residues in ^{1}H-^{15}N HSQC spectra of ubiquitin: $\delta(^{1}H^{N}$ L8)-$\delta(^{1}H^{N}$ V5), $\delta(^{1}H^{N}$ L8)-$\delta(^{1}H^{N}$ I44), $\delta(^{1}H^{N}$ L8)-$\delta(^{1}H^{N}$ H68). These differences in chemical shifts were then fitted to a linear function of the temperature. The table below summarizes the temperatures of all experiments performed in our study.

Table S1: Sample temperature for different experiments

Experiment	Field (T)	Concentration (mM)	Temperature (K)
R_1	0.5	3	296.33
R_1	0.74	3	297.09
R_1	1	3	297.20
R_1	1.4	3	296.06
R_1	2	3	296.26
R_1	3	3	296.59
R_1	5	3	296.95
R_1	14.1	0.2	296.39
R_2	14.1	0.2	296.45
NOE	14.1	0.2	296.52
η_{xy}	14.1	0.2	296.39
η_z	14.1	0.2	296.56
R_1	14.1	3	296.62
R_2	14.1	3	296.41
NOE	14.1	3	296.42
η_{xy}	14.1	3	296.64
η_z	14.1	3	296.64
R_1	18.8	3	296.38
R_2	18.8	3	296.46
NOE	18.8	3	296.38
η_{xy}	18.8	3	296.49
η_z	18.8	3	296.46

R_1	22.3	3	298.53
R_2	22.3	3	298.49
NOE	22.3	3	298.49
η_{xy}	22.3	3	298.52
η_z	22.3	3	298.51

The experiments at B_0 = 22.3 T (950 MHz for ^{1}H) were acquired at T = 298.5 K, about 2 K higher than all other experiments In order to correct for this temperature difference we used experiments at 14.1T as a reference. Using a full set of relaxation rates (R_1, R_2, NOE, longitudinal η_z and transverse η_{xy} cross-correlations) we estimated the overall correlation times at B_0 = 14.1 T and B_0 = 22.3 T. We assigned the variation of τ_c to the change of viscosity of water with temperature. Taking this effect into account, we corrected the experimental relaxation rates observed at 22.3 T prior to analysis of the relaxation rates in terms of dynamics.

3. The ICARUS protocol

ICARUS is a MATLAB package for the Iterative Correction and Analysis of Relaxation rates Under Shuttling which permits a quantitative analysis in terms of local dynamics of longitudinal relaxation rates (^{15}N R_1) recorded at a series of low magnetic fields. In order to achieve this, ICARUS is adapted from a well-known program developed for the analysis of high-field nitrogen-15 relaxation, using model-free or extended model-free spectral density functions. This package uses both ROTDIF[1] to obtain overall tumbling parameters and DYNAMICS [2] to fit microdynamics parameters (S^2, τ_c, τ_{loc}, S^2_f, τ_f).

Spectral density functions

The spectral density functions $J(\omega)$ used are:

(i) Model-free:
$$J(\omega) = \frac{S^2\tau_c}{(1+(\omega\tau_c)^2)} + \frac{(1-S^2)\tau_e}{(1-(\omega\tau_e)^2)} \quad \text{(S1)}$$

where S^2 is the generalized order parameter, τ_c the overall isotropic rotational correlation time of the molecule, and $\tau_e = \tau_c\tau_{loc}/(\tau_c + \tau_{loc})$ where τ_{loc} is a single effective correlation time that describes all internal motions.

(ii) Extended model-free: $$J(\omega) = \frac{S^2\tau_c}{(1+(\omega\tau_c)^2)} + \frac{\left(1-S_f^2\right)\tau_f^{eff}}{\left(1+\left(\omega\tau_f^{eff}\right)^2\right)} + \frac{\left(S_f^2-S^2\right)\tau_s^{eff}}{\left(1+\left(\omega\tau_s^{eff}\right)^2\right)} \quad \text{(S2)}$$

with $\tau_f^{eff} = \tau_c\tau_f/(\tau_c + \tau_f)$ and $\tau_s^{eff} = \tau_c\tau_s/(\tau_c + \tau_s)$ where τ_f (respectively τ_s) is the correlation time for fast (respectively slow) internal motions. The generalized order parameter can be expressed as a product $S^2 = S_f^2 S_s^2$ where S_f^2 and S_s^2 are generalized order parameters describing fast and slow motions. The models used in simulations of spin dynamics by ICARUS always correspond to the model selected in the previous step by DYNAMICS.

Spin System

All simulations of spin dynamics were carried out for the following spin system comprising one nitrogen-15 and 3 protons with the following distances and interactions:

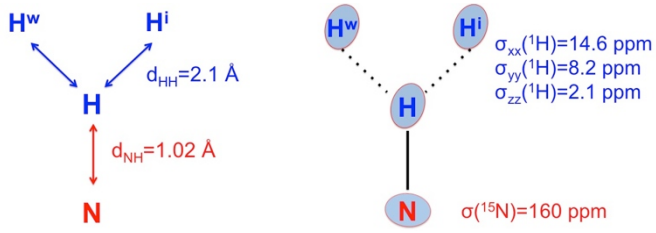

The relaxation matrix $\hat{R}$ was approximated by:

$$\hat{R} = \begin{pmatrix} 0 & 0 & 0 & 0 & 0 & 0 & 0 & 0 \\ -\theta_H & \rho_H & \sigma_{NH} & \delta_H & \sigma & 0 & \sigma & 0 \\ -\theta_N & \sigma_{NH} & \rho_N & \delta_N & 0 & 0 & 0 & 0 \\ -\theta_{NH} & \delta_H & \delta_N & \rho_{NH} & 0 & \sigma & 0 & \sigma \\ -\theta_H^i & \sigma & 0 & 0 & \rho_H^i & 0 & 0 & 0 \\ -\theta_{NH}^i & 0 & 0 & \sigma & 0 & \rho_{NH}^i & 0 & 0 \\ -\theta_H^w & \sigma & 0 & 0 & 0 & 0 & \rho_H^w & 0 \\ -\theta_{NH}^w & 0 & 0 & \sigma & 0 & 0 & 0 & \rho_{NH}^w \end{pmatrix} \quad \text{(S3)}$$

with[3]:

$$\rho_H = \frac{1}{10}c_{NH}^2\,[J(\omega_H - \omega_N) + 3J(\omega_H) + 6J(\omega_H + \omega_N)] + \frac{2}{15}\left[{c_{Hxx}}^2 + {c_{Hyy}}^2 - c_{Hxx}c_{Hyy}\right]J(\omega_H) + \frac{2}{10}c_{HH}^2[J(0) + 3J(\omega_H) + 6J(2\omega_H)]$$

$$\rho_N = \frac{1}{10}c_{NH}^2[J(\omega_H - \omega_N) + 3J(\omega_N) + 6J(\omega_H - \omega_N)] + \frac{2}{15}c_N^2 J(\omega_N)$$

$$\rho_{NH} = \frac{3}{10}c_{NH}^2\ J(\omega_N) + \frac{2}{15}c_N^2 J(\omega_N) + \frac{3}{10}c_{NH}^2 J(\omega_H) + \frac{2}{15}\left[{c_{Hxx}}^2 + {c_{Hyy}}^2 - c_{Hxx}c_{Hyy}\right]J(\omega_H) + \frac{2}{10}c_{HH}^2[J(0) + 3J(\omega_H) + 6J(2\omega_H)]$$

$$\rho_H^i = \frac{1}{10}c_{NH}^2\,[J(\omega_H - \omega_N) + 3J(\omega_H) + 6J(\omega_H + \omega_N)] + \frac{2}{15}\left[{c_{Hxx}}^2 + {c_{Hyy}}^2 - c_{Hxx}c_{Hyy}\right]J(\omega_H) + \frac{1}{10}c_{HH}^2[J(0) + 3J(\omega_H) + 6J(2\omega_H)]$$

$$\rho_{NH}^i = \frac{1}{10}c_{NH}^2[3J(\omega_N)] + \frac{2}{15}c_N^2 J(\omega_N) + \frac{1}{10}c_{NH}^2[3J(\omega_H)] + \frac{2}{15}\left[{c_{Hxx}}^2 + {c_{Hyy}}^2 - c_{Hxx}c_{Hyy}\right]J(\omega_H) + \frac{1}{10}c_{HH}^2[J(0) + 3J(\omega_H) + 6J(2\omega_H)]$$

$$\rho_H^w = \frac{1}{10}c_{NH}^2[J(\omega_H - \omega_N) + 3J(\omega_H) + 6J(\omega_H + \omega_N)] + \frac{2}{15}\left[{c_{Hxx}}^2 + {c_{Hyy}}^2 - c_{Hxx}c_{Hyy}\right]J(\omega_H) + \frac{2}{10}c_{HH}^2[J(0) + 3J(\omega_H) + 6J(2\omega_H)]$$

$$\rho_{NH}^w = \frac{1}{10}c_{NH}^2\left[3J(\omega_N) + \frac{2}{15}c_N^2 J(\omega_N) + \frac{1}{10}c_{NH}^2(3J(\omega_H))\right] + \frac{2}{15}\left[{c_{Hxx}}^2 + {c_{Hyy}}^2 - c_{Hxx}c_{Hyy}\right]J(\omega_H) + \frac{1}{10}c_{HH}^2[J(0) + 3J(\omega_H) + 6J(2\omega_H)]$$

$$\sigma_{NH} = \frac{1}{10} c_{NH}^2 [6J(\omega_H + \omega_N) - J(\omega_H - \omega_N)]$$

$$\delta_H = \frac{-4}{10}\, c_{NH}\left[c_{Hxx}\, J(\omega_H)_{xx} + c_{Hyy}\, J(\omega_H)_{yy}\right]$$

$$\delta_N = \frac{-4}{10} c_{NH} c_N J(\omega_N)_c$$

$$\sigma = \frac{1}{10} c_{HH}^2 [J(2\omega_H) - J(0)]$$

$\theta_N = \theta_H = \theta_{NH} = \theta^i_H = \theta^w_H = \theta^w_{NH} = \theta^i_{NH} = 0$;

$$J(\omega_H)_{xx} = \frac{\left[3\left(cos(\beta_{H_{xx}})\right)^2 - 1\right]}{2} J(\omega_H);\; J(\omega_H)_{yy} = \frac{\left[3\left(cos\left(\beta_{H_{yy}}\right)\right)^2 - 1\right]}{2} J(\omega_H)$$

(S4)

where $c_{NH} = \mu_0 \gamma_H \gamma_N\, h/(8\pi^2\, d_{NH}^3)$, $c_{HH} = (\mu_0 \gamma_H^2 h/8\pi^2\, d_{HH}^3$, $c_N = \Delta\sigma_N \omega_N$, $c_{H_{xx}} = \omega_H(\sigma_{H_{xx}} - \sigma_{H_{zz}})$ and $c_{H_{yy}} = \omega_H(\sigma_{H_{yy}} - \sigma_{H_{zz}})$; μ_0 is the permittivity of free space; γ_H (γ_N) is the gyromagnetic ratio of the proton (respectively of the nitrogen-15 nucleus); h is Planck's constant; ω_H (ω_N) is the Larmor frequency of the proton (respectively of the nitrogen-15); $\Delta\sigma_N$ ($= 160\times10^6$ppm) is the average value of the anisotropy of the ^{15}N chemical shift (CSA); $\sigma_{H_{xx}}$ ($= 14.6\times10^6$ppm), $\sigma_{H_{yy}}$ ($= 8.2\times10^6$ppm) and $\sigma_{H_{zz}}$ ($= 2.1\times10^6$ppm) are the main components of the ^{1}H CSA tensors; d_{NH} $(= 1.02\text{Å})$ is the internuclear nitrogen-hydrogen distance; d_{HH} ($= 2.1$ Å) is the effective distance between the proton H and the other two protons (H^i and H^w). $\beta_{H_{xx}}$ ($= 90\pi/180$) and $\beta_{H_{yy}}$ ($= 99\pi/180$) are the angles between the NH vector and the respective components of the ^{1}H CSA tensors.

First step of ICARUS

In a first step, ROTDIF and DYNAMICS are used to obtain hydrodynamic and microdynamic parameters from high-field relaxation data (^{15}N R_1, R_2 and NOE at 14.1 T. 18.8 T and 22.3 T) only (TABLE S2. see below). Using ROTDIF, the parameters of the overall rotational diffusion tensor for an axially symmetric model were estimated from relaxation rates at 14.1 T (0.2 mM or 3 mM), 18.8 T (3 mM) and 22.3 T (3 mM) (Table S2.).

Table S2: Parameters for the overall rotational diffusion tensor				
Magnetic Field	14.1 T	14.1 T	18.8 T	22.3 T*
Concentration	0.2 mM	3 mM	3 mM	3 mM
$\tau_c = (6Tr(D))^{-1}$	4.22 ± 0.15 ns	4.89 ± 0.1 ns	4.84 ± 0.2 ns	4.84 ± 0.16 ns
D_{par}/D_{per}	1.22 ± 0.08	1.22 ± 0.04	1.18 ± 0.08	1.20 ± 0.07
θ	112° ± 12°	112° ± 7°	120° ± 15°	119° ± 12°
ϕ	157° ± 29°	157° ± 15°	155° ± 36°	157° ± 27°

* Analysis carried out with temperature-corrected rates as explained in text.

Iterative analysis with ICARUS

The dynamic parameters obtained in the first step are used next to calculate the evolution of each spin system during the transfer between the high- and low-field positions as well as during the relaxation and stabilization delays (see Figure 3).

The elements of the relaxation matrix depend on the magnetic field. The transfer durations shown in table S3 and Figure S4 have been determined by using optical sensors. The position of the shuttle is described by a trajectory with a short lag time at the starting position followed by motion at a constant speed of about 11 m/s. There is an additional pre-shuttling delay of 26 ms in high field. In the simulations, the time-dependence of the populations is integrated along the trajectory from the high- to the low-field positions.

To simulate relaxation during the transfer, a time-dependent relaxation matrix is derived as a function of the position of the shuttle. The same approach is employed for relaxation during the back-transfer from the low- to the high-field position, with a somewhat lower speed, also assumed to be constant, of about 6.5 m/s. Relaxation during the stay at the low-field position is also simulated. An additional 40 ms delay accounts for the minimum duration of the stay at the low-field position. The last step is the calculation of the relaxation of the spin system during the 100 ms stabilization delay once the shuttle has returned to the high field position.

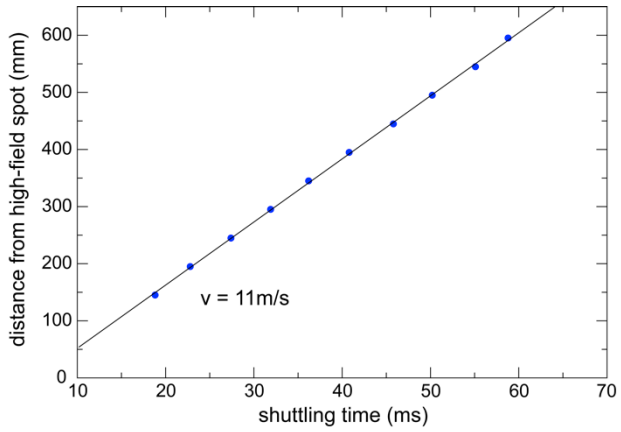

Figure S4: Correlation between the height above the high-field position and the shuttling time. The speed of the shuttle is higher for the upward motion (v = 11 m/s) than for the downward motion (v = 6.5 m/s). The correlation confirms that the velocity is constant after the initial time-lag. (In practice, relaxometry data were often recorded with slightly different pneumatic settings, which explains small variations between these data and those presented in Table S3.)

Table S3: Position and shuttling time used for simulations

B_0 (T)	Position (cm)	Shuttling time (ms)
5	27.1	41.1
3	31.1	44.1
2	34.4	46.4
1.4	37.35	48.3
1	39.8	49.9
0.75	42.55	51.6
0.5	46.2	53.7

All simulated relaxation decays were fitted to mono-exponential functions. The deviations with respect to calculated longitudinal relaxation rates of nitrogen-15 nuclei are used to correct the experimental relaxation rates. These rates are used, along with high field relaxation data (^{15}N R_1 and ^{15}N{^{1}H} NOE) as input for DYNAMICS in the subsequent steps of the ICARUS analysis.

The convergence of the analysis is fast for most residues, although up to four steps may be required for all residues to converge. The final set of microdynamic parameters is given in

Table S11. A flow-chart describing the program is shown in Figure S5.

Error evaluation

The determination of relaxation rates in low fields is more challenging than in high fields. Our analysis takes some of the complexity of the spin systems into account, with approximate evaluations of cross-relaxation pathways involving a manifold of interactions (proton-proton dipole-dipole couplings, CSA tensors…). It is unlikely that spectral noise is the main source of errors. In order to evaluate systematic errors, we implemented a jack-knife procedure. We have carried out the ICARUS analysis for 7 sets of data. Each data set included the longitudinal relaxation rates R_1 and NOE's at high fields (14.1, 18.8, and 22.3 T) as well as the longitudinal relaxation rates at 6 of the 7 low fields. Figures 4, S6-9 and Table S10 show averages of the values obtained in the 7 ICARUS analyses of the jack-knife procedure. The errors are equal to the standard deviations of these datasets multiplied by $\sqrt{(7-1)}$.

Graphical output

After the final iteration of ICARUS, the user can visualize the updated results of DYNAMICS and the latest set of corrections. Microdynamic parameters S^2 and S^2_f, τ_{loc}, $R_{ex,}$ and the model selected in DYNAMICS are indicated. In order to verify the quality of the analysis, the R_1 values that have been 'back-calculated' by ICARUS can be compared with experimental rates corrected for all residues at all fields (one figure for each field B_0). The other series of plots displays R_1 values calculated by ICARUS and corrected experimental data at all fields for all residues.

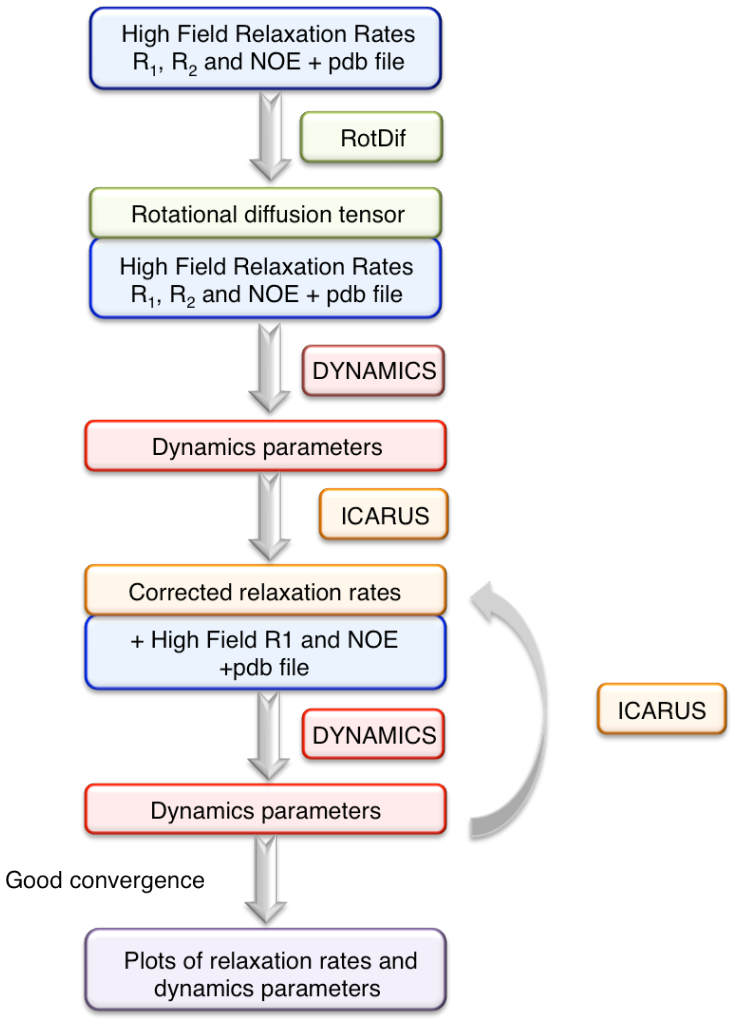

Figure S5: Flowchart for ICARUS.

4. Order parameters and timescales of motions

Order parameters

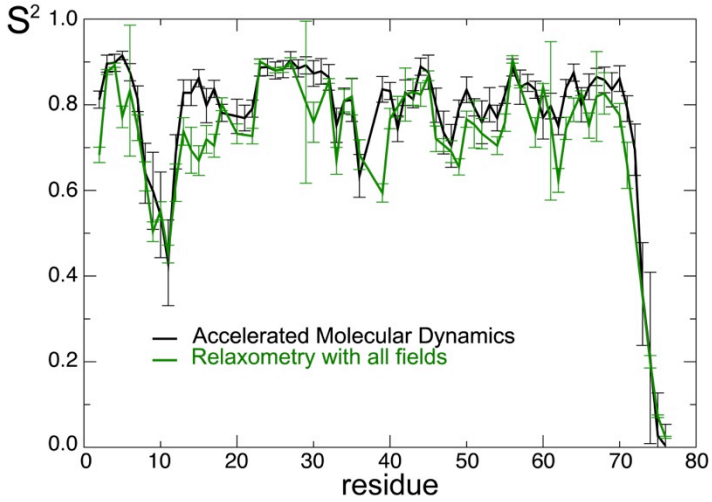

Figure S6: Comparison of order parameters in human ubiquitin. (Black) Order parameters derived from the analysis of an accelerated molecular dynamics trajectory[4]. (Green) Order parameters from the analysis of relaxation rates measured at 10 different fields.

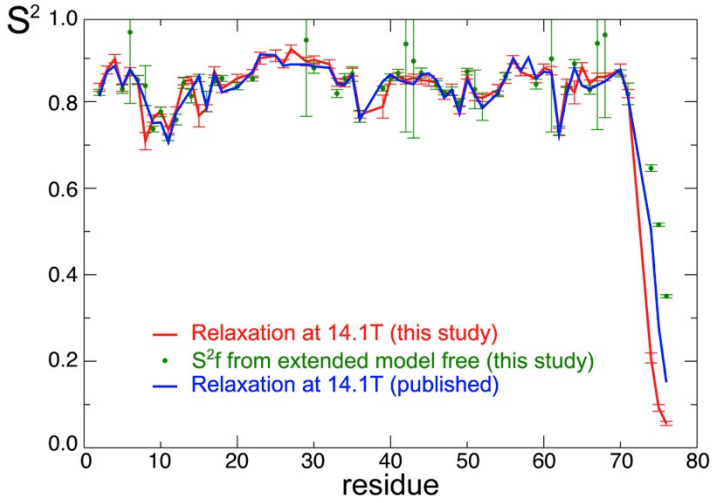

Figure S7: Comparison of order parameters in human ubiquitin. (Red) Order parameters S^2 obtained from our analysis of relaxation rates at 14.1 T only. (Blue) Order parameters derived from the analysis of a different set of nitrogen-15 relaxation rates at 14.1 T.[4] (Green) Order parameters of fast motions for an extended model-free spectral density function in the analysis by DYNAMICS of relaxation rates recorded at 14.1 T only.

Timescales of local motions

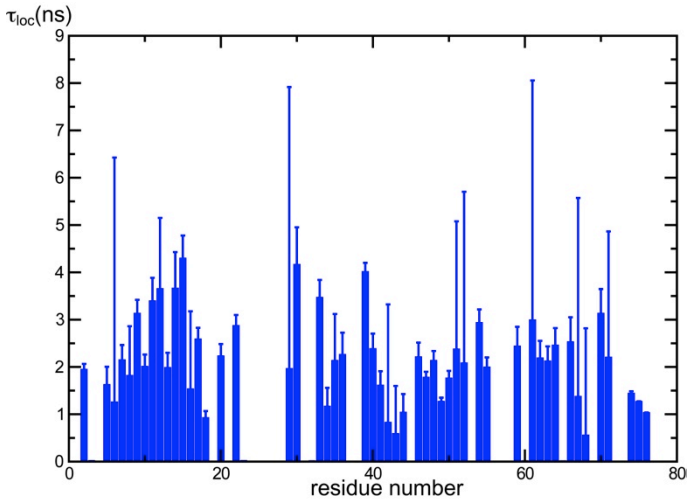

Figure S8: Timescales τ_{loc} of local motions determined by the analysis of relaxation rates measured at 10 different fields. The timescales displayed correspond either to τ_{loc} for basic model-free spectral density functions, or to τ_s for extended model-free spectral density functions. The large error bars reflect the instabilities of the selected model when applying a jack-knife analysis.

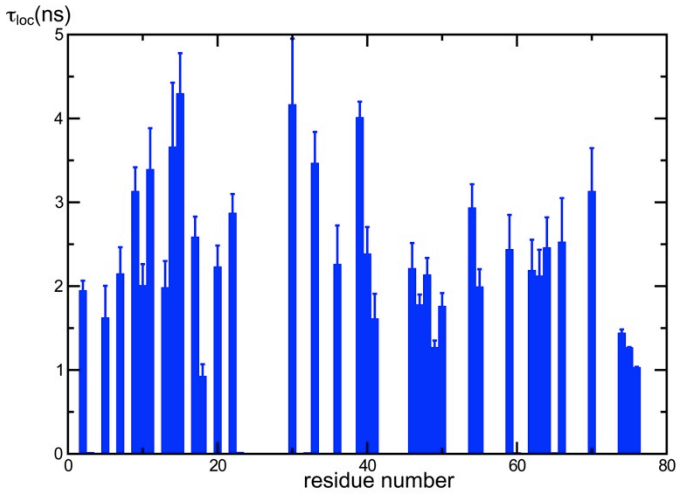

Figure S9: Timescales τ_{loc} of local motions determined by the analysis of relaxation rates measured at 10 different fields. The data are the same as in Fig. S8, we only show residues for which τ_{loc} is significant, with $\Delta\tau_{loc} < \tau_{loc}/3$.

Transverse relaxation

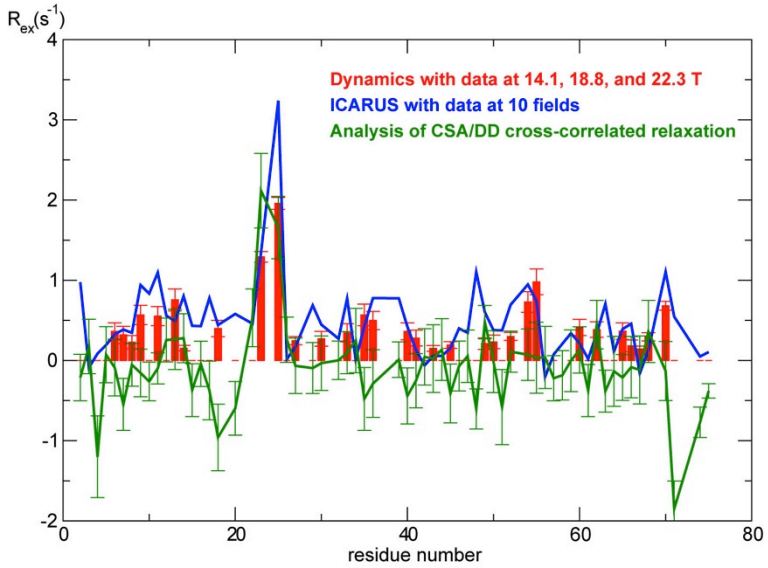

Figure S10: Contribution of chemical exchange rates R_{ex} to transverse relaxation at 14.1 T obtained with three different methods: (Green) method based on the measurement of longitudinal and transverse cross-relaxation due to cross-correlation of fluctuations of the ^{15}N chemical shift anisotropy and the dipolar coupling with the attached proton[5]; (Red) R_{ex} fitted by a conventional analysis of relaxation at 14.1, 18.8, and 22.3 T with the program DYNAMICS; (Blue) R_{ex} calculated from transverse relaxation rates with the microdynamic parameters obtained in the ICARUS analysis of relaxation rates observed at 10 magnetic fields.

Comparison of order parameters

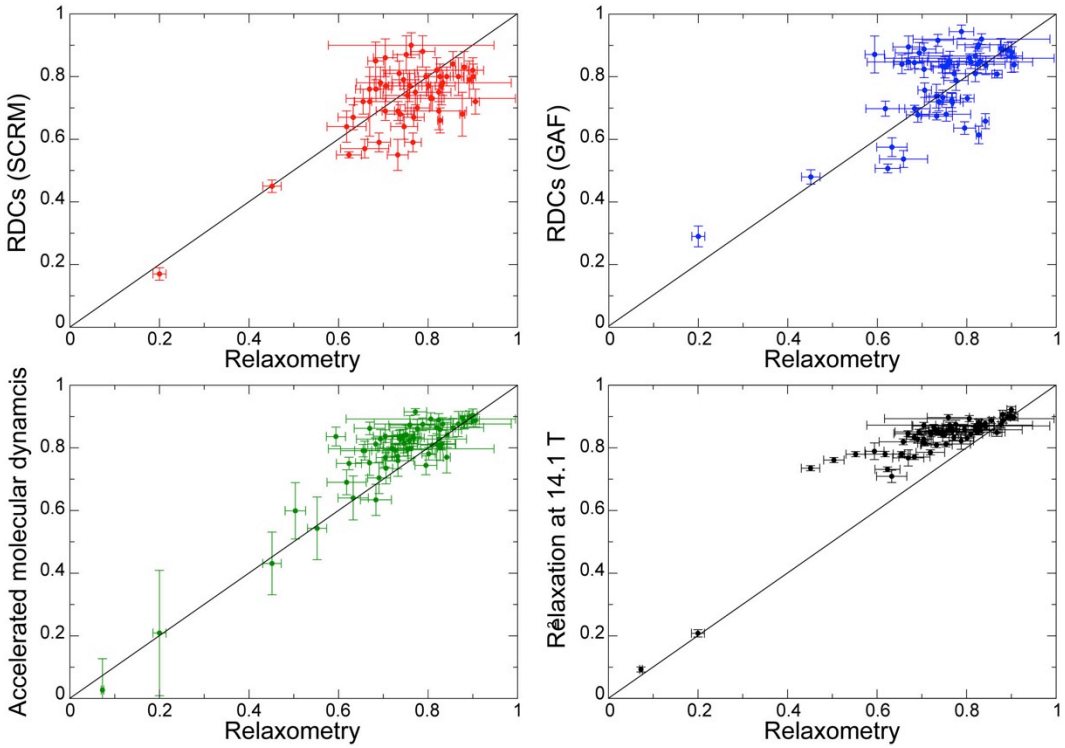

Figure S11: Comparison of the order parameters of backbone N-H vectors in ubiquitin obtained through a variety of methods. The order parameters obtained from the analysis of relaxation at 10 magnetic fields are shown on the x-axis for all plots. The y-axis displays order parameters obtained by the following methods: (a) the analysis of residual dipolar couplings measured in 23 different alignment media with the SCRM approach;[6] (b) the analysis of 36 sets of dipolar couplings with the SF-GAF approach;[7] (c) an accelerated molecular dynamics trajectory of ubiquitin;[8] and (d) our analysis of relaxation at 14.1 T.

Table S4: Statistics

	RMSD	Correlation coefficient	Regression
SCRM vs Relaxometry	0.0730	0.725	y = 0.161+0.753x
GAF vs Relaxometry	0.0771	0.660	y = 0.235+0.726x
AMD vs Relaxometry	0.0481	0.913	y = 0.086+0.948x

Effective distance to neighboring protons

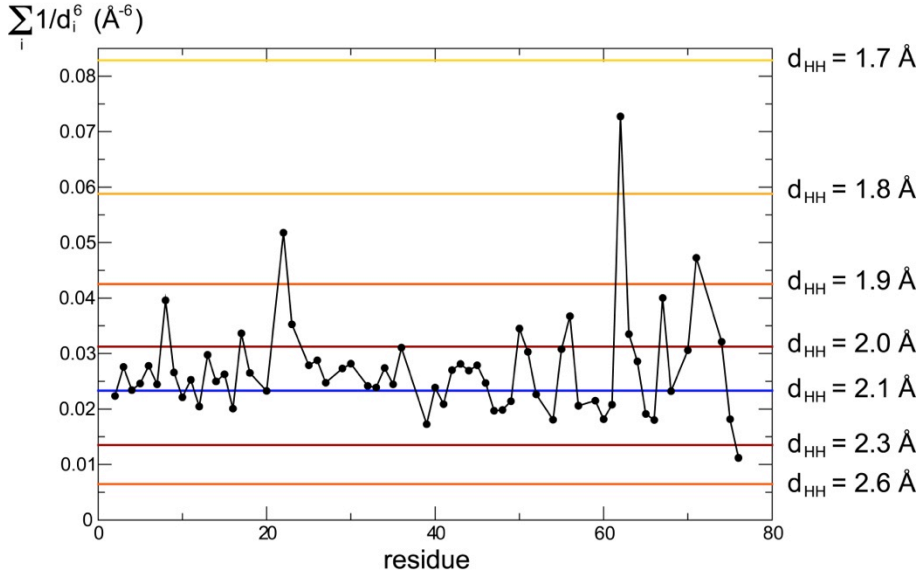

Figure S12: Total effect of proton-proton dipolar interactions for amide protons in ubiquitin. We show, for each amide proton the sum $\Sigma\ 1/d_i^6$, where d_i are the distances with all other protons in the protein (the first model in the pdb file 1d3z was used). For comparison, horizontal lines show the corresponding value $2/(d_{HH})^6$ for the effective distances in the spin system with two neighboring protons used in the ICARUS procedure:. Note that the value used in ICARUS, d_{HH} = 2.1 Å, yields $2/(d_{HH})^6 = 0.023$ Å^{-6}, which is very close to 0.025 Å^{-6}, the median of the distribution of values of $\Sigma\ 1/d_i^6$ in ubiquitin.

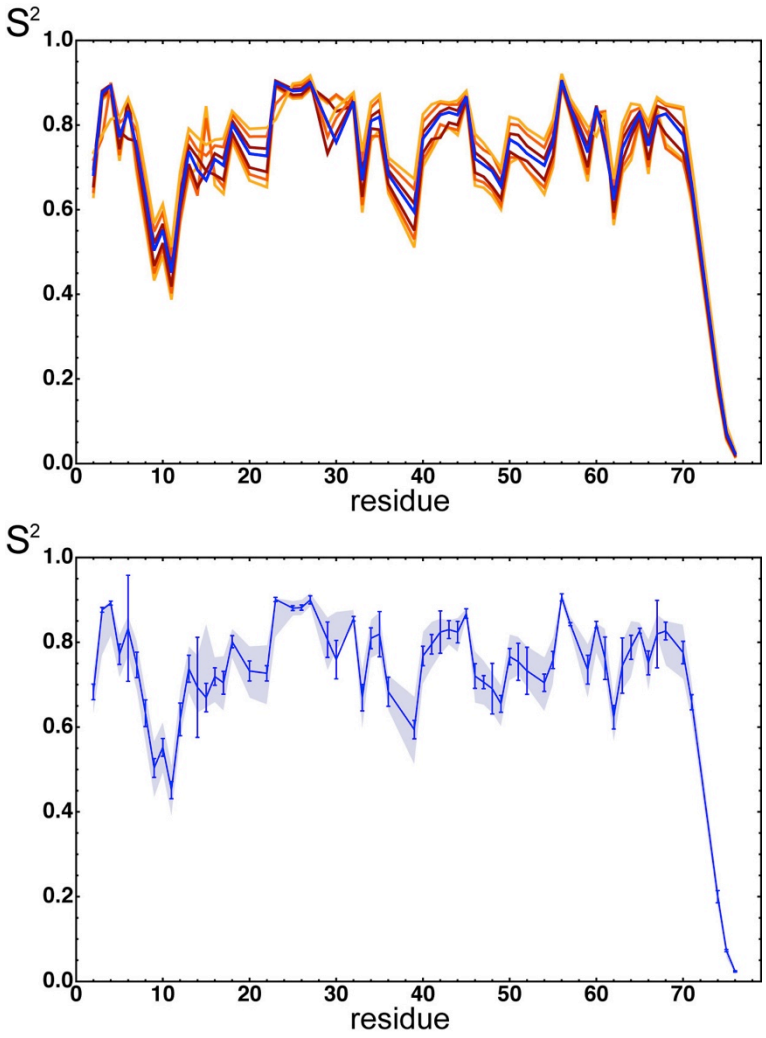

Figure S13: Dependence of order parameters upon the effective distance of neighboring protons employed in the ICARUS analysis. (Top) Order parameters obtained with d_{HH} = 2.1 Å (same as Fig. 4) are shown in purple, other curves represent order parameters obtained with d_{HH} = 1.7, 1.8, 1.9, 2.2, 2.4, and 2.6 Å. With few exceptions, the order parameters increase with increasing values of d_{HH}. (Bottom) Order parameters obtained with d_{HH} = 2.1 Å (same as Fig. 4) are shown in blue, with error intervals obtained from the jackknife analysis of ICARUS. The grey region shows the interval between the maximum and minimum order parameters obtained in the ICARUS analysis with the following values of d_{HH} = 1.7, 1.8, 1.9, 2.0, 2.2, 2.4, and 2.6 Å.

5. Relaxation data and parameters of local dynamics

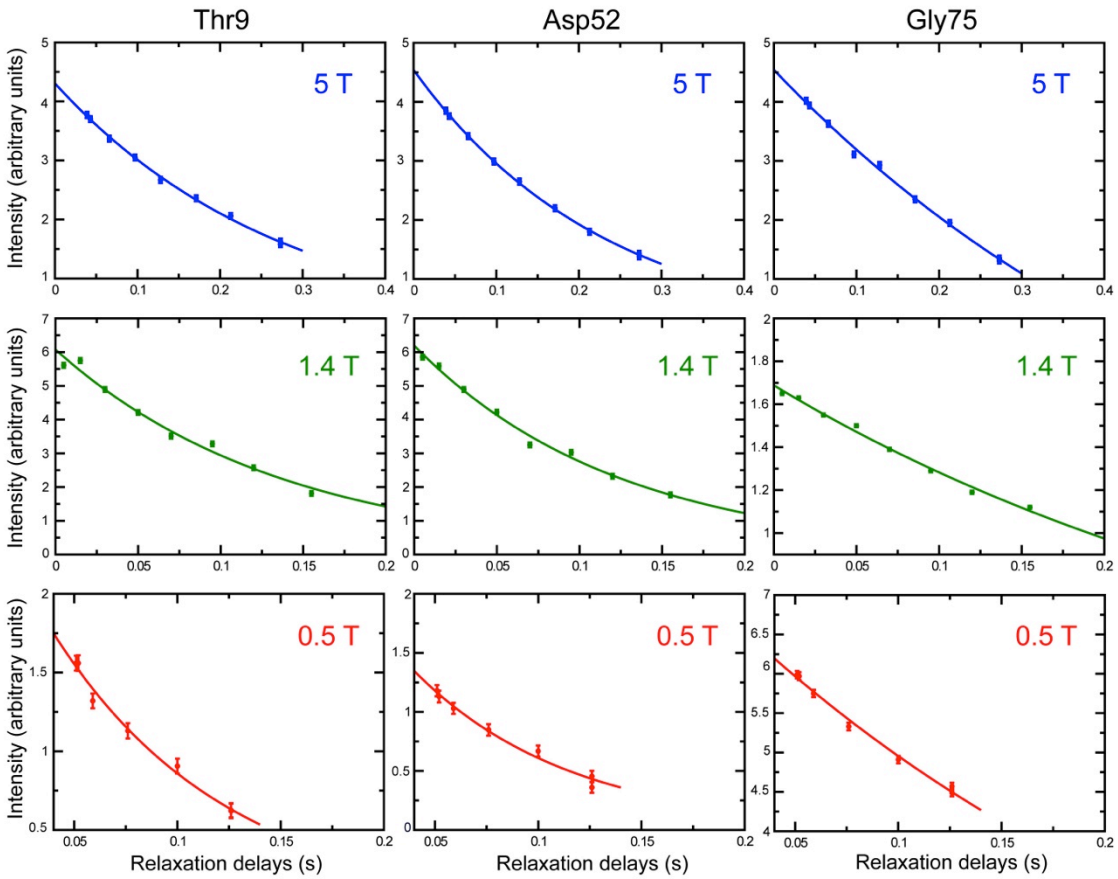

Figure S14: Relaxation decays and mono-exponential fits of a few signals at three representative magnetic fields. Results of a single relaxation experiment (total duration 11 to 13 hours) are shown for residues Thr9 (left); Asp52 (center); and Gly75 (right) at the following magnetic fields B_0^{low}: 5 T (top); 1.4 T (center); and 0.5 T (bottom). The solid lines show the results of mono-exponential fit of the relaxation decays.

Table S5: High field ^{15}N relaxation rates for 3mM ubiquitin (pH = 4.5; see table S1 for sample temperature)

	14.1 T	14.1 T	14.1 T
residue	R_1 (s^{-1})	R_2 (s^{-1})	NOE
2	1.907 ± 0.029	6.775 ± 0.102	0.731 ± 0.011
3	2.058 ± 0.031	6.752 ± 0.101	0.766 ± 0.011
4	2.106 ± 0.032	7.038 ± 0.106	0.739 ± 0.011
5	1.973 ± 0.030	6.432 ± 0.096	0.727 ± 0.011
6	2.046 ± 0.031	6.662 ± 0.100	0.766 ± 0.011
7	2.014 ± 0.030	6.604 ± 0.099	0.720 ± 0.011
8	1.986 ± 0.030	5.936 ± 0.089	0.630 ± 0.009
9	1.876 ± 0.028	5.889 ± 0.088	0.594 ± 0.009
10	1.963 ± 0.029	5.930 ± 0.089	0.588 ± 0.009
11	1.809 ± 0.027	5.787 ± 0.087	0.581 ± 0.009
12	1.863 ± 0.028	6.057 ± 0.091	0.678 ± 0.010
13	1.991 ± 0.030	6.634 ± 0.100	0.713 ± 0.011
14	1.933 ± 0.029	6.771 ± 0.102	0.774 ± 0.012
15	2.072 ± 0.031	6.528 ± 0.098	0.759 ± 0.011
16	1.832 ± 0.027	6.270 ± 0.094	0.725 ± 0.011
17	2.025 ± 0.030	6.829 ± 0.102	0.768 ± 0.012
18	1.890 ± 0.028	6.832 ± 0.102	0.706 ± 0.011
20	1.997 ± 0.030	6.702 ± 0.101	0.728 ± 0.011
22	2.057 ± 0.031	6.669 ± 0.100	0.733 ± 0.011
23	2.109 ± 0.032	8.377 ± 0.126	0.776 ± 0.012
25	2.074 ± 0.031	10.104 ± 0.152	0.759 ± 0.011
26	2.084 ± 0.031	6.900 ± 0.103	0.748 ± 0.011
27	2.126 ± 0.032	7.198 ± 0.108	0.778 ± 0.012
29	2.066 ± 0.031	6.987 ± 0.105	0.791 ± 0.012
30	2.080 ± 0.031	6.956 ± 0.104	0.751 ± 0.011
32	2.056 ± 0.031	6.952 ± 0.104	0.764 ± 0.011
33	1.965 ± 0.029	6.661 ± 0.100	0.741 ± 0.011
34	1.944 ± 0.029	6.590 ± 0.099	0.741 ± 0.011
35	1.955 ± 0.029	7.010 ± 0.105	0.762 ± 0.011
36	1.725 ± 0.026	6.399 ± 0.096	0.732 ± 0.011
39	2.048 ± 0.031	6.495 ± 0.097	0.750 ± 0.011
40	2.026 ± 0.030	6.776 ± 0.102	0.738 ± 0.011
41	2.044 ± 0.031	6.585 ± 0.099	0.731 ± 0.011
42	2.001 ± 0.030	6.534 ± 0.098	0.763 ± 0.011
43	1.992 ± 0.030	6.601 ± 0.099	0.742 ± 0.011
44	1.996 ± 0.030	6.633 ± 0.099	0.724 ± 0.011
45	2.020 ± 0.030	6.926 ± 0.104	0.729 ± 0.011
46	2.015 ± 0.030	6.472 ± 0.097	0.726 ± 0.011

47	1.934 ± 0.029	6.252 ± 0.094	0.748 ± 0.011
48	1.930 ± 0.029	6.986 ± 0.105	0.748 ± 0.011
49	1.859 ± 0.028	6.126 ± 0.092	0.656 ± 0.010
50	2.029 ± 0.030	6.713 ± 0.101	0.724 ± 0.011
51	1.880 ± 0.028	6.572 ± 0.099	0.713 ± 0.011
52	1.795 ± 0.027	6.636 ± 0.100	0.755 ± 0.011
54	1.920 ± 0.029	6.922 ± 0.104	0.748 ± 0.011
55	1.996 ± 0.030	7.020 ± 0.105	0.729 ± 0.011
56	2.124 ± 0.032	6.861 ± 0.103	0.766 ± 0.011
57	2.060 ± 0.031	6.654 ± 0.100	0.760 ± 0.011
59	2.017 ± 0.030	6.500 ± 0.098	0.767 ± 0.012
60	2.042 ± 0.031	6.783 ± 0.102	0.754 ± 0.011
61	2.035 ± 0.031	6.797 ± 0.102	0.758 ± 0.011
62	1.795 ± 0.027	5.666 ± 0.085	0.602 ± 0.009
63	1.892 ± 0.028	6.830 ± 0.102	0.754 ± 0.011
64	2.100 ± 0.031	6.659 ± 0.100	0.745 ± 0.011
65	2.036 ± 0.031	6.851 ± 0.103	0.770 ± 0.012
66	1.963 ± 0.029	6.634 ± 0.100	0.734 ± 0.011
67	2.033 ± 0.030	6.504 ± 0.098	0.791 ± 0.012
68	1.979 ± 0.030	6.683 ± 0.100	0.773 ± 0.012
70	2.072 ± 0.031	7.572 ± 0.114	0.746 ± 0.011
71	1.963 ± 0.029	6.265 ± 0.094	0.718 ± 0.011
74	1.612 ± 0.024	2.921 ± 0.044	0.091 ± 0.001
75	1.270 ± 0.019	1.924 ± 0.029	-0.319 ± -0.005
76	0.871 ± 0.013	1.295 ± 0.019	-0.785 ± -0.012

Table S5 (continued): High-field ^{15}N relaxation data for 3 mM ubiquitin (pH = 4.5; see table S1 for sample temperature)

	18.8 T	18.8 T	18.8 T
residue	R_1 (s^{-1})	R_2 (s^{-1})	NOE
2	1.458 ± 0.022	7.698 ± 0.115	0.785 ± 0.0035
3	1.575 ± 0.024	7.866 ± 0.118	0.826 ± 0.0039
4	1.617 ± 0.024	7.615 ± 0.114	0.832 ± 0.0042
5	1.490 ± 0.022	7.399 ± 0.111	0.811 ± 0.0038
6	1.580 ± 0.024	7.652 ± 0.115	0.821 ± 0.0043
7	1.552 ± 0.023	7.296 ± 0.109	0.805 ± 0.0037
8	1.575 ± 0.024	7.152 ± 0.107	0.718 ± 0.0031
9	1.514 ± 0.023	7.015 ± 0.105	0.657 ± 0.0032
10	1.534 ± 0.023	6.667 ± 0.100	0.689 ± 0.0031
11	1.482 ± 0.022	6.767 ± 0.101	0.643 ± 0.0026
12	1.474 ± 0.022	7.355 ± 0.110	0.730 ± 0.0033
13	1.554 ± 0.023	7.822 ± 0.117	0.801 ± 0.0044
14	1.482 ± 0.022	7.541 ± 0.113	0.816 ± 0.0039
15	1.584 ± 0.024	7.133 ± 0.107	0.814 ± 0.0037
16	1.360 ± 0.020	7.435 ± 0.112	0.784 ± 0.0037
17	1.533 ± 0.023	8.011 ± 0.120	0.797 ± 0.0039
18	1.418 ± 0.021	7.817 ± 0.117	0.796 ± 0.0041
20	1.539 ± 0.023	7.649 ± 0.115	0.805 ± 0.0036
22	1.579 ± 0.024	8.696 ± 0.130	0.811 ± 0.0037
23	1.660 ± 0.025	11.580 ± 0.174	0.825 ± 0.0043
25	1.610 ± 0.024	10.524 ± 0.158	0.830 ± 0.0037
26	1.623 ± 0.024	8.086 ± 0.121	0.837 ± 0.0033
27	1.609 ± 0.024	8.253 ± 0.124	0.838 ± 0.0033
29	1.577 ± 0.024	7.967 ± 0.119	0.819 ± 0.0034
30	1.618 ± 0.024	8.003 ± 0.120	0.824 ± 0.0035
32	1.590 ± 0.024	7.873 ± 0.118	0.827 ± 0.0030
33	1.522 ± 0.023	7.427 ± 0.111	0.813 ± 0.0033
34	1.506 ± 0.023	7.776 ± 0.117	0.807 ± 0.0041
35	1.496 ± 0.022	7.686 ± 0.115	0.825 ± 0.0039
36	1.330 ± 0.020	7.287 ± 0.109	0.816 ± 0.0044
39	1.585 ± 0.024	7.644 ± 0.115	0.806 ± 0.0028
40	1.569 ± 0.024	7.750 ± 0.116	0.813 ± 0.0038
41	1.549 ± 0.023	7.460 ± 0.112	0.805 ± 0.0036
42	1.480 ± 0.022	7.358 ± 0.110	0.818 ± 0.0040
43	1.485 ± 0.022	7.329 ± 0.110	0.811 ± 0.0046
44	1.547 ± 0.023	7.557 ± 0.113	0.807 ± 0.0042
45	1.546 ± 0.023	7.542 ± 0.113	0.844 ± 0.0043
46	1.560 ± 0.023	7.239 ± 0.109	0.799 ± 0.0039
47	1.478 ± 0.022	7.544 ± 0.113	0.783 ± 0.0039

48	1.502 ± 0.023	7.379 ± 0.111	0.790 ± 0.0034
49	1.477 ± 0.022	7.179 ± 0.108	0.742 ± 0.0030
50	1.595 ± 0.024	7.487 ± 0.112	0.795 ± 0.0039
51	1.444 ± 0.022	7.532 ± 0.113	0.771 ± 0.0043
52	1.352 ± 0.020	7.937 ± 0.119	0.785 ± 0.0029
54	1.482 ± 0.022	8.350 ± 0.125	0.813 ± 0.0036
55	1.538 ± 0.023	8.263 ± 0.124	0.803 ± 0.0043
56	1.637 ± 0.025	7.891 ± 0.118	0.837 ± 0.0037
57	1.582 ± 0.024	7.828 ± 0.117	0.827 ± 0.0030
59	1.553 ± 0.023	7.617 ± 0.114	0.804 ± 0.0037
60	1.571 ± 0.024	7.778 ± 0.117	0.823 ± 0.0035
61	1.593 ± 0.024	7.083 ± 0.106	0.819 ± 0.0039
62	1.403 ± 0.021	7.150 ± 0.107	0.643 ± 0.0034
63	1.442 ± 0.022	7.665 ± 0.115	0.811 ± 0.0030
64	1.596 ± 0.024	7.679 ± 0.115	0.812 ± 0.0043
65	1.580 ± 0.024	7.634 ± 0.115	0.824 ± 0.0031
66	1.459 ± 0.022	7.602 ± 0.114	0.820 ± 0.0039
67	1.525 ± 0.023	7.625 ± 0.114	0.817 ± 0.0043
68	1.499 ± 0.022	8.454 ± 0.127	0.818 ± 0.0041
70	1.558 ± 0.023	8.212 ± 0.123	0.822 ± 0.0046
71	1.526 ± 0.023	5.315 ± 0.080	0.768 ± 0.0034
74	1.448 ± 0.022	2.762 ± 0.041	0.323 ± 0.0018
75	1.242 ± 0.019	1.722 ± 0.026	0.020 ± 0.0017
76	0.852 ± 0.013	0.702 ± 0.011	-0.345 ± 0.0016

Table S5 (continued): High-field ^{15}Nrelaxation rates for 3 mM ubiquitin (pH = 4.5; see table S1 for sample temperature)

	22.3 T	22.3 T	22.3 T
residue	R_1 (s^{-1})	R_2 (s^{-1})	NOE
2	1.332 ± 0.007	8.327 ± 0.042	0.810 ± 0.008
3	1.440 ± 0.007	8.343 ± 0.043	0.850 ± 0.009
4	1.450 ± 0.007	8.630 ± 0.038	0.855 ± 0.009
5	1.307 ± 0.007	7.629 ± 0.041	0.852 ± 0.009
6	1.429 ± 0.007	8.291 ± 0.041	0.845 ± 0.008
7	1.405 ± 0.007	8.231 ± 0.037	0.824 ± 0.008
8	1.463 ± 0.007	7.468 ± 0.038	0.772 ± 0.008
9	1.398 ± 0.007	7.552 ± 0.037	0.709 ± 0.007
10	1.401 ± 0.007	7.360 ± 0.037	0.718 ± 0.007
11	1.392 ± 0.007	7.426 ± 0.036	0.704 ± 0.007
12	1.325 ± 0.007	7.277 ± 0.044	0.768 ± 0.008
13	1.391 ± 0.007	8.849 ± 0.042	0.827 ± 0.008
14	1.350 ± 0.007	8.439 ± 0.039	0.838 ± 0.008
15	1.445 ± 0.007	7.844 ± 0.037	0.842 ± 0.008
16	1.245 ± 0.006	7.462 ± 0.043	0.818 ± 0.008
17	1.382 ± 0.007	8.563 ± 0.043	0.831 ± 0.008
18	1.282 ± 0.006	8.648 ± 0.039	0.824 ± 0.008
20	1.357 ± 0.007	7.777 ± 0.041	0.832 ± 0.008
22	1.409 ± 0.007	8.249 ± 0.055	0.836 ± 0.008
23	1.509 ± 0.008	10.935 ± 0.076	0.859 ± 0.009
25	1.475 ± 0.007	15.127 ± 0.042	0.861 ± 0.009
26	1.456 ± 0.007	8.312 ± 0.046	0.850 ± 0.009
27	1.452 ± 0.007	9.134 ± 0.043	0.861 ± 0.009
29	1.422 ± 0.007	8.616 ± 0.042	0.863 ± 0.009
30	1.455 ± 0.007	8.381 ± 0.044	0.851 ± 0.009
32	1.446 ± 0.007	8.737 ± 0.041	0.857 ± 0.009
33	1.381 ± 0.007	8.281 ± 0.039	0.830 ± 0.008
34	1.348 ± 0.007	7.785 ± 0.046	0.832 ± 0.008
35	1.331 ± 0.007	9.115 ± 0.041	0.851 ± 0.009
36	1.213 ± 0.006	8.115 ± 0.040	0.852 ± 0.009
39	1.470 ± 0.007	8.001 ± 0.042	0.836 ± 0.008
40	1.406 ± 0.007	8.370 ± 0.041	0.841 ± 0.008
41	1.401 ± 0.007	8.215 ± 0.038	0.836 ± 0.008
42	1.366 ± 0.007	7.692 ± 0.041	0.837 ± 0.008
43	1.327 ± 0.007	8.114 ± 0.039	0.849 ± 0.008
44	1.348 ± 0.007	7.738 ± 0.044	0.854 ± 0.009
45	1.412 ± 0.007	8.761 ± 0.039	0.859 ± 0.009
46	1.393 ± 0.007	7.788 ± 0.037	0.818 ± 0.008
47	1.380 ± 0.007	7.357 ± 0.043	0.809 ± 0.008

48	1.387 ± 0.007	8.613 ± 0.037	0.820 ± 0.008
49	1.316 ± 0.007	7.315 ± 0.041	0.775 ± 0.008
50	1.412 ± 0.007	8.242 ± 0.040	0.832 ± 0.008
51	1.269 ± 0.006	7.906 ± 0.041	0.817 ± 0.008
52	1.234 ± 0.006	8.122 ± 0.045	0.812 ± 0.008
54	1.346 ± 0.007	8.998 ± 0.049	0.829 ± 0.008
55	1.387 ± 0.007	9.727 ± 0.043	0.828 ± 0.008
56	1.493 ± 0.007	8.547 ± 0.041	0.846 ± 0.008
57	1.472 ± 0.007	8.254 ± 0.044	0.842 ± 0.008
59	1.374 ± 0.007	7.818 ± 0.042	0.850 ± 0.009
60	1.445 ± 0.007	8.398 ± 0.042	0.843 ± 0.008
61	1.431 ± 0.007	8.329 ± 0.035	0.837 ± 0.008
62	1.293 ± 0.006	7.007 ± 0.041	0.682 ± 0.007
63	1.305 ± 0.007	8.294 ± 0.040	0.817 ± 0.008
64	1.445 ± 0.007	7.998 ± 0.042	0.851 ± 0.009
65	1.451 ± 0.007	8.433 ± 0.040	0.846 ± 0.008
66	1.327 ± 0.007	8.007 ± 0.042	0.845 ± 0.008
67	1.378 ± 0.007	8.431 ± 0.040	0.835 ± 0.008
68	1.329 ± 0.007	8.087 ± 0.052	0.841 ± 0.008
70	1.430 ± 0.007	10.393 ± 0.039	0.838 ± 0.008
71	1.413 ± 0.007	7.739 ± 0.016	0.798 ± 0.008
74	1.415 ± 0.007	3.152 ± 0.011	0.432 ± 0.004
75	1.237 ± 0.006	2.165 ± 0.007	0.181 ± 0.002
76	0.858 ± 0.004	1.432 ± 0.004	-0.196 ± 0.004

Table S6: High-field ^{15}N relaxation rates for 0.2 mM ubiquitin (pH = 4.5; see table S1 for sample temperature)

residue	14.1 T R_1 (s^{-1})	14.1 T R_2 (s^{-1})	14.1 T NOE
2	2.042 ± 0.006	5.972 ± 0.064	0.689 ± 0.020
3	2.131 ± 0.007	6.095 ± 0.072	0.700 ± 0.023
4	2.350 ± 0.009	6.556 ± 0.085	0.721 ± 0.027
5	2.103 ± 0.008	5.809 ± 0.073	0.787 ± 0.024
6	2.207 ± 0.008	5.967 ± 0.077	0.723 ± 0.024
7	2.196 ± 0.007	5.970 ± 0.070	0.711 ± 0.023
8	2.133 ± 0.006	5.402 ± 0.057	0.601 ± 0.018
9	1.906 ± 0.007	5.352 ± 0.067	0.557 ± 0.019
10	2.075 ± 0.006	5.113 ± 0.058	0.556 ± 0.018
11	1.930 ± 0.005	5.077 ± 0.049	0.587 ± 0.016
12	1.982 ± 0.006	5.433 ± 0.062	0.632 ± 0.020
13	2.155 ± 0.008	6.173 ± 0.080	0.780 ± 0.026
14	2.093 ± 0.007	5.983 ± 0.069	0.709 ± 0.022
15	2.219 ± 0.008	5.729 ± 0.071	0.718 ± 0.023
16	1.941 ± 0.006	5.556 ± 0.062	0.703 ± 0.022
17	2.171 ± 0.008	6.403 ± 0.076	0.688 ± 0.023
18	2.145 ± 0.007	5.976 ± 0.073	0.706 ± 0.023
20	2.103 ± 0.007	5.919 ± 0.067	0.692 ± 0.020
22	2.197 ± 0.007	5.757 ± 0.070	0.739 ± 0.022
23	2.278 ± 0.008	7.109 ± 0.085	0.750 ± 0.022
25	2.232 ± 0.007	8.959 ± 0.082	0.776 ± 0.022
26	2.242 ± 0.006	6.052 ± 0.060	0.742 ± 0.020
27	2.245 ± 0.007	6.637 ± 0.065	0.787 ± 0.021
29	2.183 ± 0.006	6.150 ± 0.062	0.768 ± 0.021
30	2.191 ± 0.007	6.362 ± 0.067	0.728 ± 0.020
32	2.206 ± 0.005	6.202 ± 0.052	0.741 ± 0.018
33	2.088 ± 0.006	5.883 ± 0.057	0.722 ± 0.019
34	2.063 ± 0.008	6.067 ± 0.075	0.662 ± 0.025
35	2.118 ± 0.007	6.252 ± 0.074	0.707 ± 0.021
36	1.849 ± 0.008	5.819 ± 0.092	0.670 ± 0.038
39	2.196 ± 0.005	5.768 ± 0.048	0.718 ± 0.016
40	2.168 ± 0.007	5.990 ± 0.070	0.718 ± 0.023
41	2.129 ± 0.007	5.793 ± 0.069	0.711 ± 0.023
42	2.149 ± 0.008	5.768 ± 0.074	0.802 ± 0.026
43	2.184 ± 0.009	5.742 ± 0.085	0.697 ± 0.027
44	2.161 ± 0.008	5.698 ± 0.078	0.744 ± 0.026
45	2.296 ± 0.008	6.456 ± 0.077	0.663 ± 0.024
46	2.156 ± 0.007	5.830 ± 0.071	0.660 ± 0.021
47	2.062 ± 0.007	5.677 ± 0.069	0.731 ± 0.022

48	2.060 ± 0.006	6.281 ± 0.060	0.708 ± 0.021
49	1.995 ± 0.005	5.418 ± 0.050	0.625 ± 0.018
50	2.194 ± 0.008	5.693 ± 0.075	0.748 ± 0.024
51	2.027 ± 0.008	5.857 ± 0.083	0.774 ± 0.027
52	1.921 ± 0.005	5.844 ± 0.051	0.737 ± 0.017
54	2.042 ± 0.007	6.203 ± 0.068	0.751 ± 0.023
55	2.157 ± 0.009	6.388 ± 0.085	0.737 ± 0.025
56	2.267 ± 0.008	5.988 ± 0.073	0.759 ± 0.022
57	2.211 ± 0.006	6.006 ± 0.056	0.794 ± 0.018
59	2.156 ± 0.008	5.820 ± 0.074	0.778 ± 0.025
60	2.134 ± 0.007	5.882 ± 0.064	0.702 ± 0.019
61	2.175 ± 0.007	6.058 ± 0.069	0.745 ± 0.023
62	1.891 ± 0.006	4.981 ± 0.066	0.516 ± 0.019
63	2.016 ± 0.005	5.948 ± 0.050	0.749 ± 0.018
64	2.208 ± 0.009	5.717 ± 0.080	0.719 ± 0.024
65	2.192 ± 0.006	5.942 ± 0.059	0.787 ± 0.020
66	2.086 ± 0.008	5.724 ± 0.078	0.705 ± 0.024
67	2.184 ± 0.009	5.798 ± 0.084	0.700 ± 0.024
68	2.163 ± 0.008	5.941 ± 0.077	0.732 ± 0.025
70	2.166 ± 0.009	6.689 ± 0.088	0.764 ± 0.028
71	2.115 ± 0.006	5.707 ± 0.058	0.716 ± 0.022
74	1.611 ± 0.003	2.829 ± 0.029	0.069 ± 0.012
75	1.265 ± 0.003	1.853 ± 0.028	-0.287 ± 0.012
76	0.856 ± 0.002	1.141 ± 0.022	-0.866 ± 0.013

Table S7: Uncorrected low-field ^{15}N relaxation rates for 3 mM ubiquitin (pH = 4.5; see table S1 for sample temperature)

	5 T	3 T	2 T	1.4 T
residue	R_1 (s^{-1})	R_1 (s^{-1})	R_1 (s^{-1})	R_1 (s^{-1})
2	4.169 ± 0.089	5.796 ± 0.108	7.364 ± 0.158	8.539 ± 0.151
3	4.469 ± 0.107	6.066 ± 0.128	7.598 ± 0.190	9.534 ± 0.197
4	4.531 ± 0.140	6.074 ± 0.150	7.719 ± 0.217	9.630 ± 0.258
5	4.122 ± 0.103	5.769 ± 0.127	7.453 ± 0.189	9.079 ± 0.191
6	4.418 ± 0.113	5.943 ± 0.138	7.310 ± 0.194	9.608 ± 0.218
7	4.259 ± 0.102	5.788 ± 0.118	7.744 ± 0.178	9.180 ± 0.183
8	4.025 ± 0.081	5.374 ± 0.094	6.927 ± 0.136	8.270 ± 0.125
9	3.702 ± 0.075	4.982 ± 0.084	6.179 ± 0.114	7.286 ± 0.113
10	3.672 ± 0.067	4.985 ± 0.080	6.245 ± 0.109	7.443 ± 0.112
11	3.475 ± 0.060	4.806 ± 0.067	5.759 ± 0.088	7.083 ± 0.086
12	3.779 ± 0.077	5.448 ± 0.092	6.378 ± 0.125	8.028 ± 0.132
13	4.058 ± 0.111	5.872 ± 0.136	7.345 ± 0.196	9.223 ± 0.204
14	4.206 ± 0.094	5.818 ± 0.112	7.358 ± 0.160	9.198 ± 0.168
15	4.242 ± 0.102	5.951 ± 0.125	7.259 ± 0.177	9.298 ± 0.195
16	4.156 ± 0.091	5.724 ± 0.107	7.234 ± 0.156	8.775 ± 0.156
17	4.296 ± 0.108	5.963 ± 0.132	7.637 ± 0.195	9.044 ± 0.198
18	4.476 ± 0.127	6.201 ± 0.132	7.577 ± 0.190	9.454 ± 0.204
20	4.226 ± 0.092	5.869 ± 0.107	7.233 ± 0.155	9.015 ± 0.152
22	4.335 ± 0.104	6.054 ± 0.122	7.283 ± 0.174	8.986 ± 0.176
23	4.480 ± 0.124	6.373 ± 0.159	7.368 ± 0.226	9.338 ± 0.232
25	4.568 ± 0.105	6.209 ± 0.127	7.508 ± 0.185	8.983 ± 0.182
26	4.507 ± 0.098	6.036 ± 0.117	7.586 ± 0.174	9.467 ± 0.168
27	4.669 ± 0.105	6.058 ± 0.126	7.790 ± 0.188	9.579 ± 0.184
29	4.428 ± 0.101	6.160 ± 0.126	7.853 ± 0.187	9.188 ± 0.175
30	4.753 ± 0.112	6.106 ± 0.133	7.510 ± 0.194	9.909 ± 0.195
32	4.479 ± 0.090	6.034 ± 0.108	7.557 ± 0.161	9.087 ± 0.146
33	4.090 ± 0.088	5.767 ± 0.105	7.144 ± 0.149	8.831 ± 0.148
34	4.229 ± 0.121	5.993 ± 0.142	7.535 ± 0.209	9.450 ± 0.224
35	4.258 ± 0.123	6.359 ± 0.151	8.600 ± 0.242	9.934 ± 0.234
36	3.720 ± 0.126	5.679 ± 0.113	6.940 ± 0.159	8.229 ± 0.350
39	4.162 ± 0.078	5.711 ± 0.091	7.057 ± 0.130	8.544 ± 0.124
40	4.452 ± 0.109	6.085 ± 0.130	7.600 ± 0.189	8.873 ± 0.189
41	4.351 ± 0.106	5.931 ± 0.128	7.659 ± 0.190	8.960 ± 0.188
42	4.347 ± 0.116	6.214 ± 0.137	7.530 ± 0.196	9.170 ± 0.204
43	4.436 ± 0.121	5.873 ± 0.148	7.776 ± 0.219	9.532 ± 0.240
44	4.434 ± 0.120	6.077 ± 0.148	7.874 ± 0.224	9.840 ± 0.237
45	4.206 ± 0.113	5.992 ± 0.143	7.641 ± 0.217	10.185 ± 0.239
46	4.102 ± 0.099	5.711 ± 0.120	6.980 ± 0.167	8.782 ± 0.168

47	4.128	±	0.096	5.669	±	0.115	6.932	±	0.163	8.544	±	0.160
48	4.075	±	0.084	5.627	±	0.102	7.338	±	0.148	8.785	±	0.152
49	3.831	±	0.073	5.397	±	0.087	6.941	±	0.123	7.811	±	0.114
50	4.430	±	0.119	6.142	±	0.143	7.766	±	0.213	8.868	±	0.205
51	4.224	±	0.102	5.935	±	0.138	7.445	±	0.203	9.336	±	0.219
52	4.236	±	0.078	5.847	±	0.096	7.151	±	0.135	8.602	±	0.125
54	4.166	±	0.094	5.835	±	0.115	7.053	±	0.158	8.760	±	0.166
55	4.305	±	0.119	6.082	±	0.140	7.565	±	0.204	9.161	±	0.207
56	4.490	±	0.123	6.020	±	0.148	7.577	±	0.214	10.043	±	0.220
57	4.363	±	0.091	5.966	±	0.103	7.058	±	0.141	8.986	±	0.140
59	4.293	±	0.109	5.796	±	0.133	7.347	±	0.188	9.266	±	0.198
60	4.172	±	0.098	5.675	±	0.118	7.286	±	0.176	8.711	±	0.173
61	4.489	±	0.112	5.630	±	0.131	7.687	±	0.203	9.392	±	0.193
62	3.786	±	0.086	5.192	±	0.102	6.598	±	0.141	7.869	±	0.143
63	4.359	±	0.083	5.981	±	0.096	7.574	±	0.140	9.198	±	0.130
64	4.446	±	0.131	6.203	±	0.160	7.576	±	0.238	9.757	±	0.244
65	4.159	±	0.087	5.829	±	0.104	7.080	±	0.145	8.815	±	0.145
66	4.179	±	0.106	5.800	±	0.126	7.370	±	0.182	9.020	±	0.196
67	4.304	±	0.121	5.960	±	0.149	7.404	±	0.212	9.017	±	0.223
68	4.331	±	0.118	6.142	±	0.146	7.489	±	0.205	8.743	±	0.206
70	4.452	±	0.122	6.170	±	0.150	7.849	±	0.224	9.181	±	0.225
71	4.043	±	0.078	5.357	±	0.095	7.011	±	0.139	8.357	±	0.143
74	2.425	±	0.034	3.155	±	0.033	3.844	±	0.040	4.585	±	0.038
75	1.695	±	0.027	2.216	±	0.026	2.495	±	0.028	2.897	±	0.027
76	1.106	±	0.020	1.350	±	0.018	1.442	±	0.019	1.664	±	0.018

Table S7 (continued) : Uncorrected low-field ^{15}N relaxation rates for 3 mM ubiquitin (pH = 4.5; see table S1 for sample temperature)

	1 T			0.74 T			0.5 T		
residue	R_1 (s^{-1})			R_1 (s^{-1})			R_1 (s^{-1})		
2	10.078	±	0.227	12.766	±	0.390	13.278	±	0.546
3	10.904	±	0.288	13.579	±	0.493	14.810	±	0.729
4	10.435	±	0.386	11.813	±	0.603	14.744	±	0.851
5	10.798	±	0.282	12.676	±	0.475	14.936	±	0.727
6	11.938	±	0.320	12.602	±	0.528	13.585	±	0.734
7	10.747	±	0.272	12.500	±	0.475	13.677	±	0.607
8	9.776	±	0.194	11.654	±	0.312	13.098	±	0.452
9	8.494	±	0.167	9.448	±	0.260	10.733	±	0.350
10	8.314	±	0.165	11.283	±	0.285	12.019	±	0.358
11	8.522	±	0.131	9.754	±	0.204	11.095	±	0.285
12	9.215	±	0.187	11.467	±	0.300	13.026	±	0.445
13	10.596	±	0.304	12.016	±	0.492	14.297	±	0.724
14	9.173	±	0.233	12.452	±	0.399	13.812	±	0.571
15	10.668	±	0.272	13.393	±	0.464	14.535	±	0.700
16	10.133	±	0.223	13.153	±	0.391	12.659	±	0.539
17	10.148	±	0.278	12.210	±	0.466	14.611	±	0.721
18	12.195	±	0.340	13.623	±	0.557	15.289	±	0.762
20	10.711	±	0.226	11.731	±	0.372	13.815	±	0.575
22	10.702	±	0.274	12.863	±	0.451	14.294	±	0.649
23	10.847	±	0.364	14.190	±	0.617	14.571	±	0.890
25	10.800	±	0.287	13.184	±	0.486	15.270	±	0.703
26	11.651	±	0.271	14.434	±	0.455	14.048	±	0.645
27	13.037	±	0.318	15.125	±	0.536	15.640	±	0.740
29	11.281	±	0.276	11.510	±	0.435	15.917	±	0.738
30	10.478	±	0.289	13.276	±	0.499	15.291	±	0.764
32	10.671	±	0.232	12.250	±	0.378	14.780	±	0.594
33	9.891	±	0.216	12.756	±	0.368	13.280	±	0.541
34	12.065	±	0.350	13.496	±	0.577	15.906	±	0.808
35	11.492	±	0.338	13.059	±	0.575	16.538	±	1.019
36	11.168	±	0.492	11.880	±	0.720	14.936	±	0.630
39	9.839	±	0.191	11.588	±	0.316	13.743	±	0.475
40	10.459	±	0.286	14.370	±	0.512	14.412	±	0.704
41	11.554	±	0.303	14.579	±	0.507	14.923	±	0.705
42	10.783	±	0.303	13.572	±	0.529	14.220	±	0.746
43	12.209	±	0.382	12.618	±	0.586	14.148	±	0.844
44	10.646	±	0.326	14.533	±	0.588	14.865	±	0.858
45	11.669	±	0.376	13.208	±	0.627	14.194	±	0.780
46	11.300	±	0.267	12.753	±	0.446	13.046	±	0.597
47	10.243	±	0.239	12.560	±	0.388	12.799	±	0.571

48	10.474	±	0.219	11.444	±	0.344	13.543	± 0.521
49	9.301	±	0.175	10.732	±	0.281	12.752	± 0.415
50	10.648	±	0.314	12.918	±	0.520	15.398	± 0.813
51	11.864	±	0.347	13.925	±	0.578	14.604	± 0.764
52	10.142	±	0.204	12.340	±	0.333	13.541	± 0.500
54	10.968	±	0.257	12.467	±	0.410	13.784	± 0.600
55	10.929	±	0.298	14.092	±	0.540	14.281	± 0.752
56	12.056	±	0.353	13.128	±	0.560	16.882	± 0.911
57	10.410	±	0.224	12.107	±	0.365	14.043	± 0.523
58	9.814	±	0.284	12.521	±	0.481	14.993	± 0.740
59	10.225	±	0.264	13.655	±	0.446	14.688	± 0.677
60	11.320	±	0.295	13.800	±	0.483	14.122	± 0.738
61	8.742	±	0.206	9.988	±	0.324	11.689	± 0.474
62	10.361	±	0.204	12.870	±	0.348	13.563	± 0.499
63	11.408	±	0.362	14.034	±	0.604	16.037	± 0.932
64	10.029	±	0.218	11.989	±	0.362	13.103	± 0.511
65	11.505	±	0.296	12.599	±	0.472	14.716	± 0.671
66	11.717	±	0.347	13.427	±	0.578	14.124	± 0.817
67	11.412	±	0.325	12.873	±	0.516	15.173	± 0.831
68	11.377	±	0.333	12.666	±	0.545	14.223	± 0.827
70	9.918	±	0.210	11.286	±	0.337	13.055	± 0.476
71	4.698	±	0.053	5.851	±	0.081	6.227	± 0.096
74	3.191	±	0.037	3.388	±	0.055	3.627	± 0.061
75	1.792	±	0.024	1.858	±	0.036	1.992	± 0.040
76	10.078	±	0.227	12.766	±	0.390	13.278	± 0.546

Table S8: Corrected low-field ^{15}N relaxation rates for 3 mM ubiquitin (pH = 4.5; see table S1 for sample temperature)

	5T	3T	2T	1.4T
residue	$R_1(s^{-1})$	$R_1(s^{-1})$	$R_1(s^{-1})$	$R_1(s^{-1})$
2	4.545 ± 0.097	6.089 ± 0.113	7.740 ± 0.166	9.141 ± 0.162
3	4.897 ± 0.117	6.374 ± 0.134	7.967 ± 0.199	10.204 ± 0.211
4	4.970 ± 0.153	6.384 ± 0.157	8.097 ± 0.228	10.310 ± 0.276
5	4.502 ± 0.113	6.056 ± 0.133	7.815 ± 0.198	9.708 ± 0.205
6	4.838 ± 0.124	6.250 ± 0.145	7.688 ± 0.204	10.308 ± 0.234
7	4.654 ± 0.112	6.082 ± 0.124	8.135 ± 0.187	9.830 ± 0.196
8	4.384 ± 0.089	5.653 ± 0.099	7.297 ± 0.143	8.867 ± 0.134
9	4.022 ± 0.081	5.238 ± 0.089	6.517 ± 0.120	7.820 ± 0.121
10	3.988 ± 0.073	5.242 ± 0.084	6.579 ± 0.115	7.974 ± 0.120
11	3.773 ± 0.065	5.056 ± 0.070	6.084 ± 0.093	7.612 ± 0.092
12	4.115 ± 0.084	5.719 ± 0.097	6.703 ± 0.131	8.597 ± 0.142
13	4.431 ± 0.122	6.170 ± 0.143	7.714 ± 0.206	9.873 ± 0.218
14	4.594 ± 0.103	6.112 ± 0.118	7.731 ± 0.168	9.853 ± 0.180
15	4.643 ± 0.112	6.263 ± 0.131	7.647 ± 0.186	9.987 ± 0.210
16	4.532 ± 0.099	6.007 ± 0.112	7.590 ± 0.164	9.386 ± 0.167
17	4.694 ± 0.119	6.271 ± 0.139	8.034 ± 0.205	9.694 ± 0.212
18	4.890 ± 0.139	6.510 ± 0.139	7.945 ± 0.199	10.111 ± 0.218
20	4.616 ± 0.100	6.166 ± 0.113	7.597 ± 0.162	9.651 ± 0.163
22	4.741 ± 0.113	6.366 ± 0.128	7.659 ± 0.183	9.632 ± 0.189
23	4.915 ± 0.136	6.700 ± 0.168	7.730 ± 0.237	10.000 ± 0.248
25	5.007 ± 0.115	6.524 ± 0.133	7.873 ± 0.194	9.615 ± 0.194
26	4.942 ± 0.107	6.342 ± 0.123	7.956 ± 0.183	10.133 ± 0.180
27	5.123 ± 0.115	6.368 ± 0.132	8.172 ± 0.197	10.258 ± 0.197
29	4.850 ± 0.110	6.481 ± 0.132	8.264 ± 0.197	9.863 ± 0.188
30	5.209 ± 0.123	6.423 ± 0.140	7.898 ± 0.205	10.631 ± 0.210
32	4.904 ± 0.098	6.337 ± 0.113	7.921 ± 0.168	9.720 ± 0.156
33	4.467 ± 0.096	6.062 ± 0.110	7.514 ± 0.156	9.467 ± 0.158
34	4.624 ± 0.132	6.293 ± 0.149	7.900 ± 0.219	10.108 ± 0.240
35	4.661 ± 0.135	6.682 ± 0.158	9.024 ± 0.254	10.634 ± 0.250
36	4.051 ± 0.137	5.956 ± 0.118	7.278 ± 0.167	8.794 ± 0.374
39	4.549 ± 0.085	6.013 ± 0.096	7.445 ± 0.137	9.185 ± 0.133
40	4.869 ± 0.119	6.395 ± 0.137	7.982 ± 0.199	9.502 ± 0.203
41	4.758 ± 0.116	6.231 ± 0.135	8.038 ± 0.200	9.590 ± 0.201
42	4.757 ± 0.126	6.524 ± 0.144	7.891 ± 0.206	9.806 ± 0.219
43	4.852 ± 0.133	6.165 ± 0.155	8.150 ± 0.229	10.194 ± 0.256
44	4.850 ± 0.132	6.382 ± 0.155	8.257 ± 0.235	10.527 ± 0.254
45	4.608 ± 0.123	6.295 ± 0.151	8.011 ± 0.227	10.897 ± 0.255
46	4.479 ± 0.108	6.001 ± 0.126	7.334 ± 0.175	9.404 ± 0.180
47	4.500 ± 0.104	5.953 ± 0.121	7.278 ± 0.171	9.141 ± 0.171

48	4.445	±	0.091	5.912	±	0.107	7.713	±	0.156	9.406	±	0.163
49	4.163	±	0.080	5.662	±	0.091	7.284	±	0.129	8.346	±	0.122
50	4.842	±	0.130	6.456	±	0.151	8.158	±	0.224	9.496	±	0.220
51	4.609	±	0.111	6.230	±	0.144	7.809	±	0.213	9.984	±	0.234
52	4.614	±	0.085	6.130	±	0.100	7.491	±	0.142	9.186	±	0.133
54	4.550	±	0.102	6.130	±	0.120	7.410	±	0.166	9.382	±	0.178
55	4.705	±	0.130	6.392	±	0.148	7.947	±	0.214	9.810	±	0.222
56	4.927	±	0.135	6.329	±	0.155	7.950	±	0.224	10.756	±	0.236
57	4.775	±	0.099	6.263	±	0.108	7.395	±	0.148	9.609	±	0.150
59	4.691	±	0.119	6.090	±	0.140	7.719	±	0.198	9.922	±	0.212
60	4.564	±	0.107	5.958	±	0.124	7.635	±	0.184	9.315	±	0.185
61	4.915	±	0.123	5.922	±	0.138	8.087	±	0.214	10.076	±	0.207
62	4.110	±	0.093	5.444	±	0.107	6.924	±	0.148	8.410	±	0.153
63	4.760	±	0.091	6.281	±	0.101	7.950	±	0.147	9.842	±	0.140
64	4.869	±	0.143	6.524	±	0.168	7.964	±	0.250	10.459	±	0.262
65	4.547	±	0.095	6.117	±	0.110	7.417	±	0.152	9.422	±	0.155
66	4.566	±	0.115	6.091	±	0.132	7.735	±	0.191	9.653	±	0.209
67	4.712	±	0.133	6.259	±	0.157	7.761	±	0.222	9.645	±	0.239
68	4.738	±	0.130	6.448	±	0.153	7.847	±	0.215	9.348	±	0.221
70	4.874	±	0.133	6.487	±	0.158	8.246	±	0.235	9.838	±	0.241
71	4.405	±	0.085	5.628	±	0.100	7.369	±	0.146	8.944	±	0.153
74	2.611	±	0.037	3.352	±	0.036	4.099	±	0.043	4.931	±	0.040
75	1.826	±	0.030	2.377	±	0.027	2.682	±	0.030	3.125	±	0.029
76	1.191	±	0.022	1.452	±	0.019	1.552	±	0.020	1.793	±	0.019

Table S8 (continued): Corrected low-field ^{15}N relaxation rates for 3 mM ubiquitin (pH = 4.5; see table S1 for sample temperature)

	1T			0.74T			0.5T		
residue	$R_1(s^{-1})$			$R_1(s^{-1})$			$R_1(s^{-1})$		
2	11.041	±	0.249	14.214	±	0.434	14.922	±	0.614
3	11.987	±	0.316	15.204	±	0.552	16.740	±	0.824
4	11.477	±	0.424	13.234	±	0.676	16.671	±	0.962
5	11.843	±	0.309	14.151	±	0.530	16.835	±	0.820
6	13.120	±	0.351	14.076	±	0.590	15.305	±	0.826
7	11.791	±	0.298	13.950	±	0.530	15.405	±	0.683
8	10.708	±	0.212	12.960	±	0.347	14.695	±	0.507
9	9.295	±	0.183	10.477	±	0.288	11.998	±	0.391
10	9.090	±	0.180	12.515	±	0.317	13.449	±	0.401
11	9.326	±	0.144	10.805	±	0.226	12.381	±	0.318
12	10.094	±	0.205	12.757	±	0.333	14.619	±	0.499
13	11.621	±	0.333	13.404	±	0.548	16.099	±	0.815
14	10.062	±	0.255	13.882	±	0.444	15.537	±	0.643
15	11.722	±	0.299	14.941	±	0.517	16.348	±	0.787
16	11.104	±	0.244	14.657	±	0.436	14.238	±	0.606
17	11.132	±	0.305	13.613	±	0.520	16.436	±	0.811
18	13.383	±	0.373	15.221	±	0.623	17.247	±	0.860
20	11.747	±	0.248	13.084	±	0.415	15.554	±	0.648
22	11.747	±	0.301	14.353	±	0.503	16.093	±	0.730
23	11.933	±	0.401	15.901	±	0.691	16.480	±	1.007
25	11.873	±	0.316	14.763	±	0.545	17.261	±	0.795
26	12.810	±	0.298	16.165	±	0.509	15.881	±	0.730
27	14.343	±	0.350	16.949	±	0.601	17.689	±	0.837
29	12.400	±	0.304	12.855	±	0.486	17.926	±	0.831
30	11.519	±	0.318	14.839	±	0.558	17.240	±	0.862
32	11.723	±	0.255	13.707	±	0.422	16.696	±	0.671
33	10.849	±	0.237	14.215	±	0.410	14.928	±	0.608
34	13.244	±	0.385	15.084	±	0.644	17.949	±	0.912
35	12.623	±	0.371	14.602	±	0.643	18.667	±	1.150
36	12.222	±	0.539	13.221	±	0.801	16.782	±	0.707
39	10.802	±	0.210	12.903	±	0.352	15.422	±	0.533
40	11.481	±	0.314	16.048	±	0.572	16.244	±	0.793
41	12.685	±	0.333	16.290	±	0.566	16.833	±	0.796
42	11.842	±	0.333	15.181	±	0.592	16.058	±	0.842
43	13.408	±	0.419	14.113	±	0.656	15.976	±	0.953
44	11.691	±	0.358	16.251	±	0.657	16.781	±	0.968
45	12.824	±	0.413	14.785	±	0.702	16.040	±	0.882
46	12.391	±	0.293	14.221	±	0.498	14.683	±	0.672
47	11.222	±	0.261	13.994	±	0.433	14.396	±	0.643

48	11.478	±	0.241	12.748	±	0.384	15.226	±	0.585
49	10.172	±	0.191	11.934	±	0.313	14.319	±	0.466
50	11.687	±	0.345	14.423	±	0.580	17.354	±	0.916
51	13.010	±	0.381	15.541	±	0.645	16.456	±	0.860
52	11.109	±	0.223	13.758	±	0.371	15.246	±	0.563
54	12.027	±	0.282	13.897	±	0.457	15.506	±	0.675
55	11.993	±	0.327	15.730	±	0.602	16.090	±	0.847
56	13.265	±	0.389	14.714	±	0.628	19.096	±	1.030
57	11.431	±	0.246	13.541	±	0.408	15.857	±	0.590
59	10.766	±	0.312	13.969	±	0.537	16.882	±	0.833
60	11.228	±	0.289	15.272	±	0.499	16.585	±	0.764
61	12.437	±	0.324	15.410	±	0.539	15.905	±	0.831
62	9.559	±	0.225	11.100	±	0.360	13.114	±	0.532
63	11.362	±	0.224	14.357	±	0.389	15.274	±	0.562
64	12.534	±	0.398	15.684	±	0.675	18.087	±	1.051
65	11.008	±	0.239	13.403	±	0.404	14.789	±	0.577
66	12.619	±	0.325	14.059	±	0.527	16.577	±	0.756
67	12.871	±	0.381	15.024	±	0.647	15.954	±	0.923
68	12.531	±	0.357	14.396	±	0.577	17.133	±	0.939
70	12.497	±	0.365	14.153	±	0.609	16.037	±	0.933
71	10.860	±	0.230	12.561	±	0.375	14.666	±	0.535
74	5.102	±	0.057	6.405	±	0.089	6.854	±	0.106
75	3.457	±	0.040	3.684	±	0.059	3.955	±	0.067
76	1.934	±	0.026	2.009	±	0.039	2.156	±	0.043

Table S9: Parameters of local dynamics in for 3 mM ubiquitin (pH = 4.5; see table S1 for sample temperature) derived from high-field relaxation data (14.1 T)

residue	S^2	S^2_{fast}	τ_{loc}
2	0.833 ± 0.00924	1 ±	0.02935 ± 0.00519
3	0.873 ± 0.00922	1 ±	0.00000 ± 0.00000
4	0.899 ± 0.00964	1 ±	0.04223 ± 0.01110
5	0.832 ± 0.00846	1 ±	0.02862 ± 0.00562
6	0.869 ± 0.00944	1 ±	±
7	0.851 ± 0.00937	1 ±	0.03672 ± 0.00672
8	0.709 ± 0.01968	0.8788 ± 0.0109	1.18833 ± 0.16592
9	0.761 ± 0.00821	1 ±	0.06472 ± 0.00460
10	0.779 ± 0.00850	1 ±	0.07630 ± 0.00560
11	0.735 ± 0.00802	1 ±	0.06026 ± 0.00371
12	0.779 ± 0.00851	1 ±	0.03777 ± 0.00395
13	0.848 ± 0.00865	1 ±	0.03941 ± 0.00660
14	0.851 ± 0.00805	1 ±	±
15	0.767 ± 0.02566	0.8791 ± 0.0110	3.55937 ± 0.73535
16	0.785 ± 0.00815	1 ±	0.02374 ± 0.00382
17	0.871 ± 0.00954	1 ±	0.00000 ± 0.00000
18	0.830 ± 0.00898	1 ±	0.04024 ± 0.00541
20	0.854 ± 0.00906	1 ±	0.03279 ± 0.00658
22	0.865 ± 0.00931	1 ±	0.03400 ± 0.00708
23	0.901 ± 0.01379	1 ±	±
25	0.906 ± 0.01342	1 ±	±
26	0.888 ± 0.00950	1 ±	0.02996 ± 0.00937
27	0.922 ± 0.00957	1 ±	±
29	0.893 ± 0.00975	1 ±	±
30	0.896 ± 0.00924	1 ±	±
32	0.887 ± 0.00956	1 ±	±
33	0.845 ± 0.00903	1 ±	0.02424 ± 0.00611
34	0.843 ± 0.00870	1 ±	±
35	0.868 ± 0.00905	1 ±	±
36	0.770 ± 0.00824	1 ±	0.01863 ± 0.00343
39	0.789 ± 0.02653	0.8766 ± 0.0110	2.39826 ± 0.80415
40	0.852 ± 0.01195	1 ±	0.02680 ± 0.00669
41	0.858 ± 0.00932	1 ±	0.03246 ± 0.00668
42	0.850 ± 0.00910	1 ±	0.01188 ± 0.00508
43	0.855 ± 0.00863	1 ±	±
44	0.850 ± 0.00921	1 ±	0.03352 ± 0.00668
45	0.848 ± 0.01211	1 ±	0.03094 ± 0.00636
46	0.844 ± 0.00923	1 ±	0.03185 ± 0.00626
47	0.814 ± 0.00873	1 ±	0.01669 ± 0.00468
48	0.827 ± 0.01311	1 ±	0.01873 ± 0.00526
49	0.780 ± 0.00790	1 ±	0.04624 ± 0.00403

50	0.861	±	0.00891	1	±		0.03815	±	0.00714
51	0.812	±	0.00889	1	±		0.03329	±	0.00482
52	0.809	±	0.00839	1	±			±	
54	0.827	±	0.01255	1	±		0.01866	±	0.00492
55	0.855	±	0.01247	1	±		0.03449	±	0.00704
56	0.897	±	0.00940	1	±		0.01689	±	0.00834
57	0.869	±	0.00913	1	±		0.01704	±	0.00649
59	0.853	±	0.00918	1	±			±	
60	0.878	±	0.00962	1	±			±	
61	0.872	±	0.00947	1	±		0.01890	±	0.00675
62	0.731	±	0.00751	1	±		0.05206	±	0.00326
63	0.843	±	0.00957	1	±		0.00000	±	0.00000
64	0.821	±	0.02633	0.9015	±	0.0106	1.95872	±	0.73543
65	0.881	±	0.00953	1	±			±	
66	0.842	±	0.00881	1	±		0.02788	±	0.00581
67	0.857	±	0.00902	1	±			±	
68	0.857	±	0.00921	1	±			±	
70	0.874	±	0.01295	1	±		0.02666	±	0.00802
71	0.819	±	0.00933	1	±		0.02993	±	0.00508
74	0.208	±	0.01148	0.7810	±	0.0104	1.11704	±	0.02375
75	0.092	±	0.00776	0.6871	±	0.0091	0.88851	±	0.01440
76	0.056	±	0.00466	0.5334	±	0.0079	0.66351	±	0.01104

Table S10: Parameters of local dynamics in 3 mM ubiquitin (pH = 4.5; T = 296.5 K) derived from high-field relaxation data (14.1; 18.8; and 22.3 T)

residue	S^2			S^2_f			τ_{loc}			τ_{loc}^{fast}		
2	0.836	±	0.890	0.885	±	0.546	0.759	±	0.132		±	
3	0.845	±	0.139	0.966	±	0.581	2.517	±	0.544		±	
4	0.890	±	0.187	0.924	±	0.568	1.721	±	0.516		±	
5	0.839	±	0.644	0.858	±	0.548	0.449	±	0.155		±	
6	0.756	±	0.396	0.864	±	0.134	3.444	±	0.731		±	
7	0.779	±	0.341	0.861	±	0.125	1.659	±	0.427		±	
8	0.782	±	0.238	0.882	±	0.185	1.145	±	0.158		±	
9	0.630	±	0.430	0.780	±	0.190	1.923	±	0.618	0.356	±	0.313
10	0.765	±	0.894	0.889	±	0.573	0.619	±	0.570		±	
11	0.576	±	0.482	0.761	±	0.175	2.113	±	0.442	0.337	±	0.253
12	0.899	±	0.492	1.000	±		0.346	±	0.149		±	
13	0.725	±	0.463	0.838	±	0.167	1.972	±	0.487		±	
14	0.853	±	0.623	1.000	±		0.170	±	0.144		±	
15	0.773	±	0.142	0.884	±	0.559	2.737	±	0.392		±	
16	0.772	±	0.153	0.899	±	0.770	1.545	±	0.780	0.114	±	0.269
17	0.892	±	0.516	1.000	±		0.249	±	0.249		±	
18	0.772	±	0.262	0.842	±	0.117	1.187	±	0.252		±	
20	0.867	±	0.521	1.000	±		0.172	±	0.168		±	
22	0.956	±	0.579	1.000	±		0.213	±	0.269		±	
23	0.942	±	0.778	1.000	±		0.170	±	0.469		±	
25	0.948	±	0.796	1.000	±			±			±	
26	0.919	±	0.560	1.000	±			±			±	
27	0.929	±	0.733	1.000	±			±			±	
29	0.918	±	0.536	1.000	±		0.138	±	0.241		±	
30	0.834	±	0.334	0.898	±	0.192	2.467	±	0.736		±	
32	0.874	±	0.125	0.920	±	0.563	2.177	±	0.482		±	
33	0.763	±	0.387	0.849	±	0.139	2.133	±	0.529		±	
34	0.859	±	0.543	1.000	±		0.152	±	0.178		±	
35	0.738	±	0.434	0.838	±	0.146	3.527	±	0.863		±	
36	0.673	±	0.336	0.764	±	0.129	2.297	±	0.474		±	
39	0.827	±	0.114	0.928	±	0.547	1.738	±	0.193		±	
40	0.819	±	0.323	0.872	±	0.125	1.646	±	0.532		±	
41	0.844	±	0.347	0.870	±	0.115	1.420	±	0.414		±	
42	0.854	±	0.973	1.000	±		0.963	±	0.283		±	
43	0.843	±	0.637	1.000	±		0.115	±	0.158		±	
44	0.857	±	0.674	0.887	±	0.567	0.489	±	0.155		±	
45	0.890	±	0.675	1.000	±			±			±	
46	0.841	±	0.967	0.884	±	0.537	0.783	±	0.191		±	
47	0.836	±	0.521	1.000	±		0.298	±	0.156		±	
48	0.873	±	0.533	1.000	±		0.245	±	0.200		±	
49	0.757	±	0.197	0.837	±	0.846	0.665	±	0.139		±	

50	0.893	±	0.261	0.886	±	0.159	1.298	±	0.277		±	
51	0.797	±	0.176	0.863	±	0.111	0.789	±	0.285		±	
52	0.798	±	0.673	1.000	±		0.152	±	0.915		±	
54	0.754	±	0.397	0.836	±	0.153	2.964	±	0.577		±	
55	0.797	±	0.525	0.842	±	0.185	2.322	±	0.537		±	
56	0.927	±	0.583	1.000	±			±			±	
57	0.876	±	0.170	0.984	±	0.592	1.766	±	0.457		±	
59	0.868	±	0.987	1.000	±		0.159	±	0.320		±	
60	0.786	±	0.359	0.868	±	0.119	2.958	±	0.756		±	
61	0.839	±	0.119	0.896	±	0.543	1.846	±	0.337		±	
62	0.668	±	0.320	0.749	±	0.166	1.578	±	0.677	0.356	±	0.336
63	0.855	±	0.516	1.000	±		0.135	±	0.116		±	
64	0.843	±	0.214	0.986	±	0.158	1.626	±	0.468		±	
65	0.795	±	0.359	0.872	±	0.125	3.134	±	0.782		±	
66	0.818	±	0.247	0.856	±	0.964	1.337	±	0.527		±	
67	0.866	±	0.641	1.000	±		0.158	±	0.184		±	
68	0.858	±	0.713	1.000	±		0.896	±	0.169		±	
70	0.896	±	0.756	1.000	±		0.133	±	0.253		±	
71	0.687	±	0.188	0.829	±	0.531	1.598	±	0.162		±	
74	0.197	±	0.620	0.647	±	0.428	1.457	±	0.280	0.457	±	0.145
75	0.618	±	0.396	0.513	±	0.388	1.374	±	0.294	0.518	±	0.120
76	0.948	±	0.162	0.298	±	0.685	0.495	±	0.985		±	

Table S11: Parameters of local dynamics in 3 mM ubiquitin (pH = 4.5; T = 296.5 K) derived from the analysis of relaxation data at all fields (0.5 to 22.3 T)

residue	S^2			S^2_f			τ_{loc}			τ_{loc}^{fast}		
2	0.683	±	0.179	0.822	±	0.697	1.939	±	0.125		±	
3	0.876	±	0.576	1.000	±		0.847	±	0.365		±	
4	0.892	±	0.519	1.000	±			±			±	
5	0.772	±	0.252	0.829	±	0.123	1.615	±	0.389		±	
6	0.833	±	0.153	0.967	±	0.165	1.247	±	5.179		±	
7	0.746	±	0.300	0.852	±	0.190	2.140	±	0.324		±	
8	0.633	±	0.339	0.837	±	0.470	1.888	±	1.546	0.122	±	0.280
9	0.535	±	0.229	0.737	±	0.668	3.123	±	0.295	0.319	±	0.132
10	0.553	±	0.214	0.776	±	0.113	1.999	±	0.264	0.198	±	0.334
11	0.451	±	0.267	0.716	±	0.649	3.385	±	0.499	0.323	±	0.134
12	0.618	±	0.436	0.759	±	0.122	3.643	±	1.565	0.242	±	0.244
13	0.738	±	0.322	0.843	±	0.128	1.976	±	0.324		±	
14	0.694	±	0.537	0.813	±	0.155	3.652	±	0.775		±	
15	0.670	±	0.347	0.855	±	0.855	4.288	±	0.491		±	
16	0.719	±	0.321	0.880	±	0.236	1.525	±	1.652	0.138	±	0.897
17	0.744	±	0.268	0.847	±	0.924	2.579	±	0.255		±	
18	0.812	±	0.149	0.854	±	0.666	0.917	±	0.151		±	
20	0.732	±	0.232	0.836	±	0.867	2.222	±	0.262		±	
22	0.727	±	0.182	0.853	±	0.567	2.865	±	0.235		±	
23	0.913	±	0.532	1.000	±		0.929	±	0.426		±	
25	0.885	±	0.600	1.000	±			±			±	
26	0.882	±	0.644	1.000	±			±			±	
27	0.900	±	0.994	1.000	±			±			±	
29	0.867	±	0.189	0.942	±	0.176	1.955	±	5.963		±	
30	0.759	±	0.474	0.878	±	0.122	4.157	±	0.795		±	
32	0.855	±	0.541	1.000	±		0.569	±	0.197		±	
33	0.670	±	0.314	0.819	±	0.916	3.458	±	0.386		±	
34	0.894	±	0.263	0.854	±	0.193	1.160	±	0.399		±	
35	0.819	±	0.430	0.864	±	0.169	2.127	±	0.994		±	
36	0.683	±	0.347	0.766	±	0.136	2.253	±	0.471		±	
39	0.595	±	0.214	0.837	±	0.582	4.375	±	0.196		±	
40	0.768	±	0.238	0.856	±	0.786	2.376	±	0.329		±	
41	0.795	±	0.244	0.866	±	0.926	1.629	±	0.358		±	
42	0.824	±	0.621	0.933	±	0.234	0.818	±	2.552		±	
43	0.830	±	0.386	0.894	±	0.178	0.578	±	1.217		±	
44	0.824	±	0.275	0.867	±	0.113	1.394	±	0.396		±	
45	0.868	±	0.114	1.000	±			±			±	
46	0.723	±	0.298	0.839	±	0.994	2.230	±	0.312		±	
47	0.759	±	0.152	0.821	±	0.531	1.772	±	0.129		±	
48	0.695	±	0.256	0.825	±	0.948	2.128	±	0.299		±	

49	0.655	±	0.190	0.800	±	0.818	1.270	±	0.962		±	
50	0.766	±	0.188	0.869	±	0.733	1.753	±	0.164		±	
51	0.754	±	0.548	0.828	±	0.448	2.366	±	2.712	0.122	±	0.256
52	0.733	±	0.354	0.789	±	0.318	2.740	±	3.629	0.457	±	0.140
54	0.745	±	0.268	0.818	±	0.647	2.926	±	0.290		±	
55	0.758	±	0.256	0.859	±	0.775	1.984	±	0.218		±	
56	0.958	±	0.857	1.000	±			±			±	
57	0.843	±	0.322	1.000	±			±			±	
59	0.735	±	0.345	0.845	±	0.115	2.428	±	0.421		±	
60	0.842	±	0.784	1.000	±		0.636	±	0.334		±	
61	0.762	±	0.185	0.899	±	0.169	2.983	±	5.792		±	
62	0.623	±	0.280	0.732	±	0.148	2.180	±	0.374	0.342	±	0.145
63	0.745	±	0.259	0.826	±	0.966	2.114	±	0.321		±	
64	0.788	±	0.275	0.888	±	0.956	2.450	±	0.378		±	
65	0.827	±	0.564	1.000	±		0.522	±	0.158		±	
66	0.751	±	0.295	0.827	±	0.177	2.519	±	0.538		±	
67	0.819	±	0.149	0.935	±	0.199	1.367	±	4.264		±	
68	0.827	±	0.484	0.954	±	0.191	0.549	±	2.268		±	
70	0.776	±	0.273	0.866	±	0.838	3.123	±	0.524		±	
71	0.658	±	0.538	0.818	±	0.255	2.194	±	2.669	0.285	±	0.136
74	0.200	±	0.146	0.646	±	0.773	1.433	±	0.517	0.442	±	0.130
75	0.726	±	0.295	0.515	±	0.389	1.258	±	0.146	0.496	±	0.752
76	0.237	±	0.233	0.353	±	0.370	1.233	±	0.142	0.384	±	0.695

6. References

(1) Walker, O.; Varadan, R.; Fushman, D. *J. Magn. Reson.* **2004**, *168*, 336.

(2) Fushman, D.; Cahill, S.; Cowburn, D. *J. Mol. Biol.* **1997**, *266*, 173.

(3) Cavanagh, J.; Fairbrother, W. J.; Palmer III, A. G.; Rance, M.; Skelton, N. J. *Protein NMR Spectroscopy: Principles and practice*; 2nd edition, Academic Press: San Diego, 2006.

(4) Salmon, L.; Bouvignies, G.; Markwick, P.; Blackledge, M. *Biochemistry* **2011**, *50*, 2735.

(5) Kroenke, C. D.; Loria, J. P.; Lee, L. K.; Rance, M.; Palmer III, A. G. *J. Am. Chem. Soc.* **1998**, *120*, 7905.

(6) Lakomek, N. A.; Walter, K. F. A.; Fares, C.; Lange, O. F.; de Groot, B. L.; Grubmuller, H.; Bruschweiler, R.; Munk, A.; Becker, S.; Meiler, J.; Griesinger, C. *J. Biomol. NMR* **2008**, *41*, 139.

(7) Salmon, L.; Bouvignies, G.; Markwick, P.; Lakomek, N.; Showalter, S.; Li, D. W.; Walter, K.; Griesinger, C.; Bruschweiler, R.; Blackledge, M. *Angew. Chem.-Int. Edit.* **2009**, *48*, 4154.

(8) Markwick, P. R. L.; Bouvignies, G.; Salmon, L.; McCammon, J. A.; Nilges, M.; Blackledge, M. *J. Am. Chem. Soc.* **2009**, *131*, 16968.